Synthetic alkyl-ether-lipid promotes TRPV2 channel trafficking trough PI3K/Akt-girdin axis in cancer cells and increases mammary tumour volume

Maxime Guéguinou, Romain Felix, Séverine Marionneau-Lambot, Thibauld Oullier, Aubin Penna, Sana Kouba, Audrey Gambade, Yann Fourbon, David Ternant, Christophe Arnoult, et al.

Synthetic Alkyl-Ether-lipid promotes TRPV2 Channel trafficking trough PI3K/Akt-Girdin Axis in cancer cells and increases mammary tumor volume.

Maxime Guéguinou [1-2], Romain Felix [1], Séverine Marionneau-Lambot [8], Thibault Oullier [7], Aubin Penna [5], Sana Kouba [1], Audrey Gambade [1], Yann Fourbon[1], David Ternant[2], Chirstophe Arnoult [2], Gaelle Simon [3], Ana Maria Bouchet [1], Aurélie Chantôme [1], Thomas Harnois [5], Jean Paul Haelters [3], Paul Alain Jaffrès [3], Gunther Weber [1], Philippe Bougnoux [1], François Carreaux [6], Olivier Mignen [4], Christophe Vandier[1,†] and Marie Potier-Cartereau [1,†,*]

[1] Inserm UMR 1069, Nutrition Croissance Cancer, Faculté de Médecine, Université de Tours, F-37032, France.

[2] PATCH Team, EA 7501 GICC, Faculté de Médecine, Université de Tours, F-37032, France.

[3] CNRS, CEMCA, UMR CNRS 6521, UFR Sciences et techniques, Université de Bretagne Occidentale, Brest, F-29238, France.

[4] Inserm UMR 1227 Immunothérapies et Pathologies lymphocytaires B, CHU Morvan, Université de Bretagne Occidentale, Brest, F-29609, France.

[5] STIM Team, ERL CNRS 7349, UFR SFA Pole Biologie Santé, Université de Poitiers, F-86073, France.

[6] UMR CNRS 6226, Institut des Sciences Chimiques de Rennes, Université de Rennes, F-35700, France.

[7] Inserm UMR 1235 TENS, Faculté de Médecine, Université de Nantes, F-44035, France

[8] Therassay Module 8, IRS-UN, Université de Nantes, F-4400, France.

[*] Correspondance: Marie Potier-Cartereau, marie.potier-cartereau@univ-tours.fr; Tel.: +33 247366152; Fax: +33-247-366-226.

[†] Marie Potier-Cartereau and Christophe Vandier contributed equally to this work

Highlights

What is already known

- Transient Receptor Potential Vanilloid type 2 (TRPV2) can be activated by lipids and is implicated in several cancers.
- Alkyl-ether-lipids have anti-tumour properties.

What this study adds

- Alkyl-ether-lipids modulate TRPV2 trafficking and cancer cells.

What is the clinical significance?

- This study highlights the potential modulation of TRPV2 by alkyl-ether-lipids as a novel avenue for research in the treatment of metastatic cancer to directly target the primary tumour or to potentiate a chemotherapeutic agent.

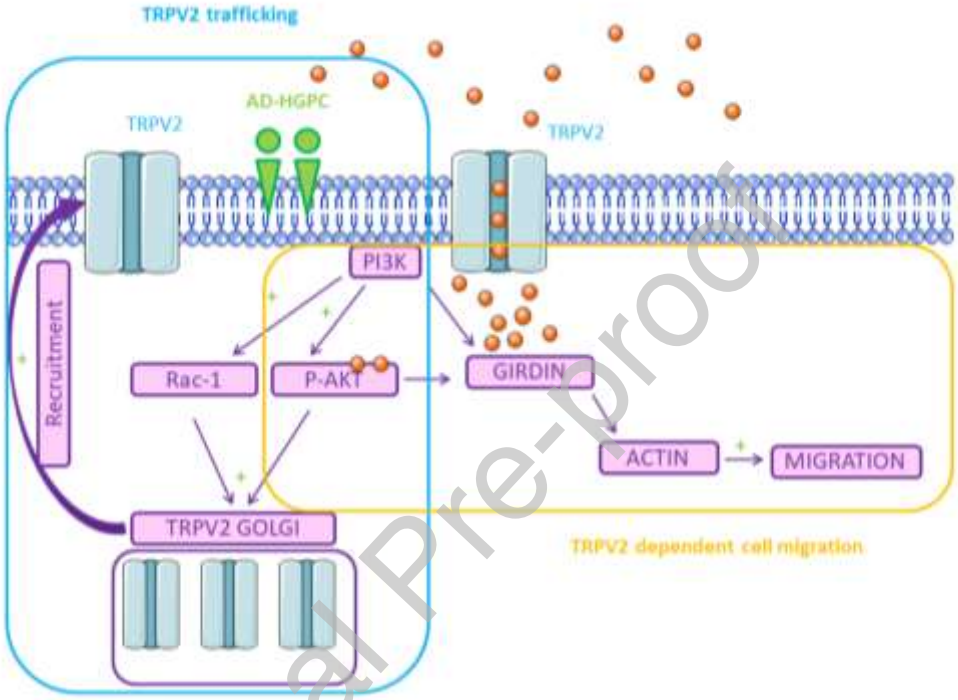

Graphical abstract
Hypothetical schema represent TRPV2 trafficking induced by AD-HGPC. AD-HGPC activates PI3K/Rac1 GTPases and the PI3K/Akt pathway and induces translocation of TRPV2 to the plasma membrane by Golgi vesicle transport.

Abstract

The Transient Receptor Potential Vanilloid type 2 (TRPV2) channel is highly selective for Ca^{2+} and can be activated by lipids, such as LysoPhosphatidylCholine (LPC). LPC analogues, such as the synthetic alkyl-ether-lipid edelfosine or the endogenous alkyl-ether-lipid Platelet Activating Factor (PAF), modulates ion channels in cancer cells. This opens the way to develop alkyl-ether-lipids for the modulation of TRPV2 in cancer. Here, we investigated the role of 2-Acetamido-2-Deoxy-l-O-Hexadecyl-rac-Glycero-3-PhosphatidylCholine (AD-

HGPC), a new alkyl-ether-lipid (LPC analogue), on TRPV2 trafficking and its impact on Ca^{2+} -dependent cell migration. The effect of AD-HGPC on the TRPV2 channel and tumour process was further investigated using calcium imaging and an *in vivo* mouse model. Using molecular and pharmacological approaches, we dissected the mechanism implicated in alkyl-ether-lipids sensitive TRPV2 trafficking. We found that TRPV2 promotes constitutive Ca^{2+} entry, leading to migration of highly metastatic breast cancer cell lines through the PI3K/Akt-Girdin axis. AD-HGPC addresses the functional TRPV2 channel in the plasma membrane through Golgi stimulation and PI3K/Akt/Rac-dependent cytoskeletal reorganization, leading to constitutive Ca^{2+} entry and breast cancer cell migration (without affecting the development of metastasis), in a mouse model. We describe, for the first time, the biological role of a new alkyl-ether-lipid on TRPV2 channel trafficking in breast cancer cells and highlight the potential modulation of TRPV2 by alkyl-ether-lipids as a novel avenue for research in the treatment of metastatic cancer.

Keywords: TRPV2; constitutive Ca^{2+} entry; alkyl-ether-lipid; breast cancer cell migration

1. Introduction

TRPV2, the second member of the transient receptor potential vanilloid family of ion channels, is composed of homotetramers, each subunit having six transmembrane segments, with the S5–S6 segments defining the pore and selectivity filter with high selectivity for Ca^{2+}> Mg^{2+}> Na^{+} ~Cs^{+} ~K^{+} [1]. The C-terminus contains the TRP domain important for phosphatidylinositol 4,5-bisphosphate [2] and CaM binding [3]. The N-glycosylation motif between the S5–S6 loop is required for TRPV2 plasma membrane localization. This is because only the glycosylated form reaches the cell's surface, while the non-glycosylated form remains in the cytosol [4]. The physiological role of TRPV2 differs among the various tissues where it is expressed. In the nervous system, TRPV2 has been proposed to have a role in neural development, in nociception and in various osmosensory mechanisms, including osmotic balance, autonomous regulation and somatosensation [5, 6]. Outside the nervous system, TRPV2 participates in cardiac Ca^{2+} regulation and contractility [7] and has also been implicated in the endocrine system (more specifically in pancreatic insulin secretion) [8] and in the immune system [9-11]. TRPV2 channels have been detected at the intercalated discs of myocardiocytes, which are critical for detecting the mechanical forces generated by contraction and have been described to increase osteoclast differentiation under acidosis [12]. In epithelial cancer cells, TRPV2 has been shown to be specifically implicated in the

proliferation of glioblastoma cells [13] and in the progression of prostate cancer and bladder cancer (BC) toward more invasive phenotypes (for review see [14]). TRPV2 expression is increased in high-grade and high-stage urothelial cancer tissues and cell lines [15]. TRPV2 activation increases the intracellular calcium levels, decreases cell viability and induces apoptotic death of BC cell lines [16]. Furthermore, Liu et al. have shown that TRPV2 mediated migration and invasion through metalloproteinase-2 activation in BC cancer cell lines [17]. Other studies have found a role for adrenomedullin (calcitonin family of peptides) in stimulating TRPV2 and indirectly promoting tumour progression and metastasis. Adrenomedullin induces prostate and urothelial cancer cells migration and invasion through TRPV2 translocation to the plasma membrane and subsequent increase in resting calcium level [18]. More recently, TRPV2 was proposed as a biomarker and therapeutic target in patients with triple negative and oestrogen receptor alpha negative breast cancers [19].

Cannabis sativa derivatives have been described as potent activators of TRPV2 [20]; moreover, probenecid (an activator) and tranilast (an inhibitor) [21, 22] are two compounds with better selectivity towards TRPV2 channels. TRPV2 was found to be modulated by lipids, such as endogenous LPC, that activate TRPV2 channels, thus increasing the invasiveness of prostate cancer cells [23]. This activation is dependent on the length of the side chain and the nature of the lysophospholipid head group. TRPV2-mediated calcium uptake stimulated by LPC occurs via Gq/Go-protein and phosphatidylinositol-3,4 kinase (PI3,4K) signalling [23]. The literature to date is also scarce as to the role of LPC in TRPV1 function. Nonetheless, it has been suggested that TRPV1 activation is partly responsible for LPC-induced monocyte migration. However, the molecular mechanisms by which LPC produces its effects on monocyte function are not understood [24]. Interestingly, we found that LPC analogues, such as the synthetic alkyl-ether-lipid edelfosine or the endogenous alkyl-ether-lipid Platelet Activating factor (PAF), modulate ion channels in cancer cells [25, 26]. Edelfosine has a longer half-life than LPC due to an aliphatic chain linked *via* an ether bond in the *sn-1* position of glycerol, instead of the esterified and hydrolysable fatty acid for LPC. First, studies on alkyl-ether-lipids in cancer quantified the global alkyl-ether-lipid contents in the tissues of patients, leading to the general conclusion that tumours contain more alkyl-ether-lipids than non-tumour tissues [27], but presently, we do not know why. Alkyl ether lipids have many roles in cancer, including anti-tumour properties [28, 29], and they can reduce the side effects of radiotherapy [30]. Interestingly, we showed that the synthetic alkyl-ether-lipid Ohmline was found to target the potassium ion channel, leading to a decrease in potassium current, constitutive calcium entry, cell migration and development of bone metastasis [31].

So, this opens the way to develop alkyl-ether-lipids for ion channel modulation, such as the lysophospholipid-sensitive TRPV2 channel, in cancers.

Here, we investigated the effect of a synthetic alkyl-ether-lipid on the migration of TRPV2-dependent breast cancer cells and its impact on tumour development. We show that TRPV2 works as a constitutive active channel in breast cancer cell lines and promotes constitutive Ca^{2+} entry-dependent cell migration through the activation of the PI3K-girdin axis. An immunohistochemical analysis of clinical breast cancer samples revealed the significance of our *in vitro* observations: tumours of the G2–3 stage stained positive for TRPV2 whereas G0–1 tumours did not. This strongly emphasizes the clinical consistency of our observations. In parallel, we synthesized a LPC analogue by replacing the sn-1 ester bond with an ether linkage and by replacing the hydroxyl group at the sn-2 position with an acetamido group to generate 2-Acetamido-2-Deoxy-l-O-Hexadecyl-rac-Glycero-3-PhosphatidylCholine (AD-HGPC). These structural modifications likely hamper its metabolization by either acyltransferases or lysophospholipases. We found that AD-HGPC activates the TRPV2 channel, leading to constitutive Ca^{2+} entry and breast cancer cell migration through TRPV2 translocation to the plasma membrane induced by the PI3K/Akt/Rac1 signalling pathway without affecting the development of metastasis in a mouse model.

2. Methods

2.1 Cell Lines and Reagents

The human breast cancer cell lines MDA-MB-435s, MDA-MB-231 (triple negative breast cancer cells) and MCF-7 (ER+, PR+, HER2-) were obtained from the American Type Culture Collection (LGC Promochem, Molsheim, France) and maintained in alpha-MEM (for MDA-MB-435s cells) or DMEM (for MCF-7 and MDA-MB-231 cells) supplemented with 5% foetal bovine serum, without antibiotics at 37°C in 95% (v/v) air/5% (v/v) CO_2. Human embryonic kidney 293T cell (HEK-293T) controls and TRPV2 have been obtained from Dr. Aubin Penna, ERL 7368 CNRS Université de Poitiers. HEK controls and HEK-hTRPV2 were cultured in DMEM supplemented with 10% of foetal bovine serum. LY294002 and MK2206 were purchased from Sigma Aldrich (Sigma Aldrich, Saint Louis, MI, USA). Tranilast and AD-HGPC (under its racemic form) were used following reported procedures [32, 33].

2.2 Immunohistochemistry

The breast invasive ductal carcinoma tissue microarray BR1503d (US Biomax Inc., Rockville, MD) was used to assess TRPV2 expression. Immunohistochemical staining was performed on a Discovery Automated IHC stainer (Roche ®, Illkirsh, France). Slides were stained using the validated HPA044993 anti-TRPV2 Prestige Antibodies® (Sigma Aldrich, Saint Louis, MI, USA) at a dilution of 1:200 for 60 min at 37°C. Signal enhancement was performed using the Ventana ChromoMap Kit slides (biotin-free detection system). Sections were counterstained with haematoxylin and mounted with DPX mounting medium. Histological information, including TNM, clinical stage and pathology grade, was obtained with the array. An Anatomopathologist was done a detailed pathological assessment of each sample who also performed *blinded* manual *scoring*. Individual tumour regions were analysed and scored for TRPV2 expression (None/low/medium/high), taking into account both the intensity and number of positives cells.

2.3 In Vivo Model

Mice (Janvier Laboratories, Le Genest-Saint-Isle, France) were bred and housed in the *in vivo* platform of Cancéropôle Grand Ouest. All animal studies were approved by the institutional Animal Care (licence care C44-278 approved on 12/16/2015) and Use Committee at the University of Nantes F-44000 France (Legislation and Ethics files #2837 approved on 03/01/2016. For the mammary fat pad (MFP) model, female NMRI/nude mice, 4-weeks old, were used. The mice were anesthetized by intraperitoneal 100 mg/kg ketamine plus 10 mg/kg xylazine administration and a right fat pad was cleared. Subconfluent MDA-MB-435s-luc cells were harvested, washed in PBS, and 2 x 10^6 cells were injected in a volume of 50 µL of PBS into the cleared fat pad. Tumour volumes were calculated using the formula: length x width x depth. The mice were treated two times a week for 15 weeks with tranilast (50 mg/kg), AD-HGPC (0.1 mg/kg) or vehicle (vehicle (0.6‰ ethanol/0.4‰ dimethyl sulfoxide) administered *intraperitoneally.* Primary tumours were removed when the volume reached 900 mm^3. In control animals, we did not observe any adverse effects from the administration of tranilast or AD-HGPC (no compartmental, weight growth abnormalities or liver and heart toxicities were observed after necropsy). The materials and methods used for bioluminescence imaging (BLI) have been described previously [34]. Briefly, all of the mice were assessed weekly using whole-body BLI to quantify relative amounts of tumour burden and metastases (Φimageur TM; BIOSPACE Lab). Each mouse was given 150 mg/kg body weight of D-luciferin potassium salt (Interchim, Montluçon, France) by intraperitoneal injection and anesthetized with ketamine/xylazine injection as above. Bioluminescence images were

acquired 3–5 min after injection and were collected in real-time until the saturation plate was reached in the lateral, ventral and dorsal positions. The photon counts emitted by the tumour and metastases were performed by a photon imager system. Regions of interest were drawn around the MFP tumour and metastases. The amount of tumour burden was quantified as the relative amount of photons produced from the luciferase activity in cells and expressed in cpm using the software Photovision+ (version 1.3; Biospace Lab). At necropsy, the *ex vivo* BLI measurement for each collected organ was performed within 15 min after injection with D-luciferin.

A generalized logistic model was used to describe the increase of tumour volume across time. This model included four parameters: initial volume measurement (V0), first-order growth rate constant (kgrowth), maximum tumour volume (Vmax), and power coefficient γ. Model parameters were estimated using nonlinear mixed-effects modelling. This approach allowed us to describe the inter-subject variability in the population (mean and inter-subject standard deviations) and to quantify the association of factors of variability (referred to as covariate, with an inter-subject distribution of Gomperz parameters. Indeed, the influence of treatment (AD-HGPC or tranilast) was tested as a covariate on both kgrowth and Vmax. This analysis was carried out using MonolixSuite2019 (Lixoft®, Antony, France). The effect of treatment on each parameter was tested using the likelihood ratio test (LRT).

2.4 Cell Migration

Cell migration was analysed in 24-well plates receiving 8-µm pore size polyethylene terephthalate membrane cell culture inserts (Becton Dickinson, Rungis, France), as previously described [35]. Briefly, 4×10^4 cells were seeded in the upper compartment with medium culture supplemented with 5% FBS (± drugs/high external Ca^{2+} concentration). The lower compartment was filled with medium culture supplemented with 5% FBS (± drugs/high external Ca^{2+} concentration). Two-dimensional migration assays were performed without coating. After 24 h, stationary cells were removed from the top side of the membrane, whereas cells that had migrated to the bottom side of the inserts were fixed. Then, the nuclei were stained and automatically counted [36]. At least three independent experiments were performed, with each of them in triplicate.

2.5 Constitutive Ca^{2+} Entry Measurements

Cells were loaded in Petri dishes for 45 min at 37°C with the ratiometric dye Fura2-AM (5 mmol/L). Then, the cells were trypsinized, washed with Opti-MEM Reduced Serum

Medium, GlutaMax (Life-Technologies, Carlsbad, CA, USA), and centrifuged (800 x *g* for 5 min). Immediately after centrifugation, cells were resuspended at 1 x 10^6 cells in 2 mL PSS Ca^{2+}-free solution. Fluorescence emission was measured at 510 nm with an excitation light at 340 and 380 nm (Hitachi FL-2500). PSS Ca^{2+}-free solution containing (in mM) NaCl, 140; $MgCl_2$, 1; KCl, 4; EGTA, 1; D-glucose, 11.1; and HEPES, 10, adjusted to pH 7.4 with NaOH, was used.

2.6 Electrophysiology

Electrophysiological recordings were performed in the whole-cell configuration of the patch clamp technique, as already described [25]. Briefly, patch pipettes (2.0–4.0 MΩ) were filled with a pipette solution containing (in mM) KCl, 145; $MgCl_2$, 1; Mg-ATP, 1; HEPES, 10; $CaCl_2$, 0.87 and EGTA, 1, adjusted to pH 7.2 with KOH, pCa6. Whole-cell macroscopic currents in HEK293T-TRPV2 cells were measured using a ramp protocol from +100 mV to −100 mV, with a holding potential of 0 mV (500 ms duration; 4 s intervals). The current amplitudes of TRPV2 channels were analysed at +100 mV. Voltage clamp protocols were generated and the data captured with a computer using a Digidata 1200 interface, Axopatch 200B amplifier and pClamp9 software (Axon Instruments, USA). The analysis was carried out using Clampfit 9 and Origin 6 software (Microcal Software, Northampton). The physiological saline solution (PSS) contained (in mM) NaCl 140, MgCl2 1, KCl 4, CaCl22, D-glucose 11.1 and HEPES 10, adjusted to pH 7.4 with NaOH.

2.7 Transfection Assay

Briefly, 2.5 x 10^5 MDA-MB-435s and MDA-MB-231 breast cancer cells/well were plated in 6-well plates in Opti-MEM supplemented with 5% FBS without antibiotics. Cells were incubated with a mix of siRNA (20 nM) and lipofectamine in medium without serum for 6 h. After incubation, an equal volume of medium with serum was added to each well. The siRNA sequences directed against TRPV2 were purchased from EurogenTech (Liège, Belgium). siGelsolin (sc-37330) or siGirdin (sc-94984) were purchased from Santa Cruz Biotechnologies (Santa Cruz, CA, USA). For control siRNA, we used the following sequences (Invitrogen): 5'CUGUAUCGAAUGUUAUGAGCC3' [37] and 5'GCUCAUAACAUUCGAUACAG3' [37]. Experiments were performed 48 h after transfection. pEGFP Rac1N17 and pEGFP were transfected in MDA-MB-435s cells with lipofectamine 2000 (Invitrogen, Carlsbad, CA, USA), according to the manufacturer's protocol.

2.8 Confocal Microscopy

MDA-MB-231 and MDA-MB-435s cells were cultured on glass for 24 h, then treated with AD-HGPC and LPC in Dulbecco's modified Eagle's medium containing 5% foetal calf serum for 10 min. Cells were then fixed for 10 min in 3.7% paraformaldehyde and permeabilized by incubation for 10 min in 0.1% triton-X-100 in phosphate-buffered saline at room temperature. Unspecific sites were saturated by incubating them for 30 min with 3% bovine serum albumin and 3% normal goat serum in phosphate-buffered saline. TRPV2 was stained by incubating the cells for 60 min with TRPV2 antibody (ACC-039, Alomone, Jerusalem, Israel). F-actin was stained by incubating the cells for 60 min with Alexa Fluor 594 phalloidin (1/200, Invitrogen, Carlsbad, CA, USA) and Alexa Fluor 488 (1/2000). Fluorescent images were captured with a JAI camera (model CV-M4+CL), with the use of an automated filter wheel coupled to a Leica DMRB fluorescence microscope (Leica Microsystems).

2.9 Western Blot Experiments

The antibodies used were the following: rabbit anti-TRPV2 (ACC-039), mouse anti-Gelsolin (sc-398244, Santa Cruz Biotech Santa Cruz, CA, USA), rabbit anti-Girdin (Sc-133371 Santa Cruz Biotech, Santa Cruz, CA, USA), rabbit anti-GAPDH (D16H11, Cell Signaling, Danvers, MA, USA), rabbit phospho-Akt (Ser473) and total Akt (Cell Signaling, Danvers, MA, USA) and horseradish peroxidase conjugated anti-rabbit or anti-mouse (Jackson Immuno-Research Laboratories, West Grove, PA, USA). Rabbit anti-Girdin S1416 Phosphorylated (IBL Code No. 28067, Takasaki-Shi, Japan).

RacGTPase Activity

Recombinant Proteins:

The GST-PAK-CRIB domains were obtained as pGEX-2 T fusion genes (gift of JG Collard, Netherlands Cancer Institute, Amsterdam, NL, USA) and produced as described [38]. Recombinant proteins were prepared as glutathione S-transferase fusion proteins in *Escherichia coli* (BL21 strain), purified using glutathione-sepharose beads (Amersham Pharmacia Biotech, Little Chalfont, UK), and used as GST-fusion proteins.

Affinity binding assay:

A total of 10^7 cells were washed twice in cold PBS and then lysed in 1 mL of lysis buffer (Tris-HCl 50 mM, pH 7.4, NaCl 100 mM, MgCl2 2 mM, 1% N P-40 (w/v), and 10% glycerol, containing protease cocktail inhibitor 1X). Lysates were mixed into 50 µL of GST-fusion protein (GST-PAK-CD) corresponding to 5 mg of protein bound to glutathione-sepharose beads. Incubation was conducted at 4°C overnight. Bead-bound complexes were washed four times in the lysis buffer, boiled in Laemmli sample buffer and fractionated by a 13% SDS–PAGE, followed by Western blotting. For the PAK-CD assay, the presence of Rac1 was revealed using anti-Rac1 antibodies clone 23A8 (05-389 Upstate, Millipore, Burlington, MA, USA).

2.10 Flow Cytometry Experiments

Cells were incubated at 4°C with saturating concentrations of TRPV2 antibody (1:100 Alomone, Jerusalem, ISR, ACC-039) in the dark for 30 min, washed twice with PBS, fixed in 0.1% Azide-PBS-4% FBS solution. For intracellular staining, cells were washed with cold PBS then incubated for 20 min with 100 µL Cytofix/Cytoperm™Fixation/Permeabilization Kit (BD Biosciences, Rungis, France). Cells were incubated with rabbit anti-TRPV2 antibody for 1 h at 4°C, washed, and then incubated with an anti-rabbit antibody coupled to an Alexa Fluor 647 for 45 min at 4°C. HEK 293 T cells were used as negative control. We used the protein transport inhibitor GolgiStop™ (554724 BD, Rungis, France). All flow cytometry (FCM) analyses were performed with a minimum of 5000 events using a Gallios flow cytometer and Kaluza version 1.2 (Beckman Coulter, Villepinte, France).

3. Statistics

Statistical analyses were performed using SigmaStat software (Systat Software, Inc). Unless otherwise indicated, data were expressed as mean ± standard error of the mean (N, number of experiments and n, number of cells from independent experiments). For comparison between more than two means, we used the Kruskal-Wallis one way analysis of variance followed by Dunn's or Dunnet's post hoc tests, as appropriate. Comparisons between two means were made using the Mann-Whitney t-test. Differences were considered significant when $p < 0.05$.

4. Results

4.1 TRPV2 Promotes Constitutive Ca^{2+} Entry and Migration of Breast Cancer Cells

To study the expression of TRPV2 in epithelial breast cells, we performed Western blot and immunocytochemical experiments and found that the TRPV2 channel was solely expressed in MDA-MB-435s, MDA-MB-231 (triple negative breast cancer cells) and MCF-7 (ER+, PR+, HER2-) cancer cell lines but not in the non-cancerous MCF-10A cell line (Figure 1A). Interestingly, TRPV2 antibody demonstrated a functional effect on TRPV2, as it decreased migration of MDA-MB-435s and MDA-MB-231 cells (Figure 1B). To investigate the role of TRPV2 in the migratory ability of cancers cells, TRPV2 was knocked down using siRNA or inhibited by tranilast (pharmacological inhibitor). In both breast cancer cell lines, silencing of TRPV2 and tranilast decreased cell migration (Figure 1C–E), without affecting cell viability (Supplemental data Figure 1A). Since we have demonstrated that breast cancer cell migration is regulated by constitutive Ca^{2+} ~~influx~~ entry (CCE) [31], we evaluated the role of TRPV2 in breast cancer CCE and showed that both TRPV2 silencing and its inhibition by tranilast reduced CCE (Figure 1F, G). To demonstrate a possible link between CCE and cancer cell migration, we depolarized cells with 40 mM KCl (a condition for which we have already demonstrated that plasma membrane was more positive, reducing the driving force for Ca^{2+} entry) [34]. As expected, the decrease of driving force for Ca^{2+} entry decreased Ca^{2+} entry and the migration of cancer cells (Figure 1H, I and Supplemental data Figure 1B). Thus, we demonstrated that the migration of breast cancer cells is regulated by the TRPV2 channel that is constitutively active in these cells.

4.2 TRPV2 Channel Promotes Breast Cancer Cell Migration through the PI3K-Girdin Axis

To investigate molecular mechanisms by which TRPV2-dependent CCE regulates cell migration, we studied the role of the Ca^{2+}-sensitive protease calpain, a master regulator of cell migration. Figure 2A shows that TRPV2 silencing or treatment with tranilast did not modify the calpain activity of breast cancer cells (Supplemental data Figure 1C). Nevertheless, the quantity of actin polymerization was changed (Figure 2B), suggesting the involvement of actin-binding proteins, such as girdin, which has been involved in cell migration [39]. Figure 2C shows that silencing girdin decreased the migration of MDA-MB-435s cancer cells. To go further into the molecular mechanisms by which TRPV2 regulates cell migration, we studied the implication of the PI3K/Akt pathway, since girdin is a PI3K/Akt substrate that plays an important role in actin organization and Akt-dependent cell migration [40]. Figure 2D shows that both Akt (Left panel) and girdin phosphorylation (Right panel) were decreased following TRPV2 silencing. Furthermore, inhibition of Akt phosphorylation by MK2206 decreased migration of MDA-MB-435s cancer cells (Figure 2E). These results showed that the

constitutive TRPV2 Ca^{2+} channel promotes migration of breast cancer cells by regulating the PI3K-girdin axis (Figure 2F). Taken together, our data show the involvement of the constitutively active TRPV2 channel in migration of breast cancer cell. This could suggest a role of this channel in breast cancer cell progression.

4.3 TRPV2 expression is correlated with high histologic grade of breast cancer and tranilast decreases development of metastases in vivo

The expression pattern of TRPV2 was examined in normal and breast cancer tissues by tissue microarray (TMA) according to clinical grade/stage (Figure 3Aa). We observed that TRPV2 was significantly highly expressed in G2–3 breast cancer tissues compared to G0–1 tissues, suggesting an association of its expression with breast cancer progression ($p < 0.05$) (Figure 3Ab). To confirm the role of the TRPV2 channel in breast cancer cell progression, we used a metastatic breast cancer mouse model that already was developed [25]. Mice were treated with either vehicle or tranilast (Figure 3B). As shown in Figure 3C, tranilast had no effect on primary tumour volume (a non-significant trend toward a decrease in the Vmax in the presence of tranilast is observed (Vmax = 662 mm^3, $p = 0.30$), while there was a significantly reduced development of metastases (Figure 3D, right panel). Indeed, metastatic tissues were detected in all vehicle-treated mice (10/10), whereas 4/10 of mice treated with tranilast did not present with any signs of metastases *ex vivo* (Figure 3D, left panel). Thus, this suggests a major role for TRPV2 in the development of metastases and breast cancer progression.

4.4 A New Synthetic Alkyl-Ether-Lipid Activates TRPV2 Channel Leading to Ca^{2+} Entry and Cell Migration

LPC has been demonstrated to activate TRPV2 and to promote prostate cancer cell migration [23]. We observed that LPC increased migration of MDA-MB-435s cells (Figure 4A), an effect that is prevented by the suppression of TRPV2 (Figure 4A). Likewise, the alkyl-ether-lipid AD-HGPC promoted MDA-MB-435s cell migration (Figure 4A), albeit at lower concentration (300 nM) compared to LPC (1 µM). This effect was prevented by silencing TRPV2 (Figure 4B). It should be note that cell viability was not affected by AD-HGPC (Supplemental data Figure 1E). Interestingly, AD-HGPC increased the amplitude of the CCE (Figure 4C) as observed with LPC (Supplemental data Figure 1F). *In vivo*, the estimated mean (interindividual standard deviation) of model parameters were V0 = 33.1 mm^3 (1.19), kgrowth = 0.16 day^{-1} (0.21), Vmax = 933 mm^3 (0.69) and $\gamma = 0.13$ (–). This showed

that tumour volume was doubled in 4.3 days in mean and that means Vmax was 933 mm^3. Treatment was not significantly associated with kgrowth, but Vmax was significantly increased in the presence of AD-HGPC (Vmax = 1943 mm^3, p = 0.039) (Figure 4Da). AD-HGPC had no effect on the development of metastases (Figure 4Db). To confirm that the biological effects of AD-HGPC involved the TRPV2 channel, we performed the same experiments in an HEK293 cell line that overexpressed human TRPV2 (HEK293-hTRPV2). As expected, both LPC and AD-HGPC increased the migration (Figure 4E, left panel) and CCE of HEK293-hTRPV2 cells (Figure 4E, right panel) while having no effect on HEK293 wild type cells (Figure 4E). Using the patch-clamp technique, the effects of LPC and AD-HGPC were tested on the amplitude of TRPV2 current in HEK293-hTRPV2 cells. Correspondingly to the results obtained in Ca^{2+} imaging and migration assays, both LPC and AD-HGPC increased the amplitude of TRPV2 currents (Figure 5A, B). This effect was blocked by lanthanum (La^{3+}), a well-known inhibitor of Ca^{2+} entry. These results demonstrated the ability of LPC and AD-HGPC to activate TRPV2 channels, probably leading to the increase of CCE and cancer cell migration. Moreover, Figure 5C shows that both LPC and AD-HGPC started to increase TRPV2 currents 2 min after their application, with a maximal effect obtained 5 min after the application of the compounds. Taken together, these results suggest that the effects of AD-HGPC on TRPV2 could be due to an increase of channel translocation to the plasma membrane, as previously observed in LPC-treated prostate cancer cells [23].

4.5 AD-HGPC Induces TRPV2 Translocation to the Plasma Membrane through PI3K/Akt/Rac1 Signalling Pathway

To evaluate the possible plasma membrane translocation of TRPV2 protein from the intracellular pool following treatment with AD-HGPC, we quantified plasma membrane TRPV2 channels using a TRPV2 antibody recognizing the extracellular side of the channel. As shown in Figure 6A, treatment with AD-HGPC increases the cell surface expression of TRPV2 channels in MDA-MB-435s cells, which is also observed with LPC. Identical results were obtained with MDA-MB-231 cells (Supplemental data Figure 1G). Following these results, we investigated the role of amphiphilic compounds (LPC and AD-HGPC) on TRPV2 trafficking through Golgi in HEK293-hTRPV2 cells. Figure 6B shows that the increase of TRPV2 translocation induced by LPC or AD-HGPC was prevented by a Golgi blocker. While under control conditions, where most of the TRPV2 channels were localized in the intracellular compartment, AD-HGPC helps in the recruitment of TRPV2 to the plasma

membrane through the activation of Golgi cisternae. Since we demonstrated a role for TRPV2 in Akt activation (Figure 3D), we wondered whether Akt was involved in TRPV2 translocation following stimulation with AD-HGPC. First, we performed immunofluorescence assays to measure the PI3K activity by the Btk-PH-GFP fusion protein. As shown in Figure 6C, in HEK293-hTRPV2 cells, AD-HGPC induces the translocation of PI3K to the plasma membrane. Acute stimulation by AD-HGPC leads to the translocation of Btk from the cytoplasm to the plasma membrane (bottom left panel), and pharmacological inhibition of PI3K by LY294002 prevented this translocation (bottom right panel), with a diffuse localization of Btk-PH-GFP. In addition, pharmacological inhibition of the PI3K/Akt pathway by LY294002 and MK2206 reduced TRPV2 cell surface expression (Figure 6D, E). Identical results were obtained in HEK-hTRPV2 cells (Supplemental data Figure 2A). Interestingly, these blockers decreased migration of MDA-MB-435s cells (Figure 6F). Moreover, 10 min of AD-HGPC stimulation enhanced Akt phosphorylation expression in both MDA-MB-435s and HEK293-hTRPV2 cells (Figure 6G). Altogether, these data show the ability of the alkyl-ether-lipid AD-HGPC to enhance TRPV2 translocation through Akt, leading to an increase in the migration capacity of breast cancer cells. To further explore the mechanism of action of AD-HGPC, we examined the involvement of small GTPases Rac1 in TRPV2 translocation. Rac1 was found to regulate vesicular transport and protein trafficking by reorganization of the cytoskeleton. In HEK293-hTRPV2 cells, inhibition of Rac1 by a dominant-negative plasmid (pRacN17-GFP) blocked the translocation of TRPV2 to the plasma membrane (Figure 7A). Moreover, the increase of TRPV2 translocation with AD-HGPC was abolished by the PI3K inhibitor LY294002 and the inhibition of Rac1 by pRacN17-GFP abolished the effect of PI3K on TRPV2 translocation. Correspondingly, expression of Rac1-GTP was decreased by the PI3K inhibitor alone and was associated with AD-HGPC stimulation (Figure 7B). Thus, all these data suggest that both PI3K/Rac1 GTPase and PI3K/Akt pathways induce the translocation of the TRPV2 channel to the plasma membrane by Golgi vesicle transport (see graphical abstract).

5. Discussion

Many reports have proven the important functions of TRPV2 in tumour progression, and some studies have shown that TPRV2 may be clinically associated with cancer [41, 42], particularly in the urinary tract [43-45]. Its expression levels have been correlated with the tumour stage and severity of urothelial carcinoma of the human bladder [15]. In 2010, Monet et al. established a role for TRPV2 in prostate cancer progression to the aggressive castration-

resistant stage, encouraging the evaluation of TRPV2 as a potential prognostic marker and therapeutic target in the setting of advanced prostate cancer [46]. In the present study, we examined the capability of TRPV2 activation and translocation to induce the migration of breast cancer cells. We have demonstrated an endogenous expression of TRPV2 channels in breast cancer cell lines. In active bone resorptive lacunae observed during the development of bone metastases in breast cancer, extracellular Ca^{2+} concentration could be as high as 8 to 40 mmol/L, whereas in the vicinity of the unaltered bone surface, it is normally closer to 2 mmol/L [47]. We have previously shown that CCE was essential for breast cancer cell migration and development of bone metastases [31].

TRPV2 generates constitutive Ca^{2+} influx and promotes Ca^{2+}-dependent cell migration, without increasing the activity of Ca^{2+} sensitive protease calpain, through PI3K signalling. Gelsolin plays an important role in actin dynamics and its activity depends on Ca^{2+}. Gelsolin binds to pre-existing actin filaments and caps them in the presence of micromolar Ca^{2+} and is consequently displaced by interactions with regulatory phospholipids, such as phosphatidylinositol-4,5-bisphosphate [48]. Gelsolin activity is necessary for cell migration in podosome-like structure formation through PI3K signalling [49, 50]. Moreover, Nagasawa and Kojima demonstrated the translocation process of TRPV2 to the podosomes in a mouse macrophage cell line [51]. Podosomes are highly dynamic actin-rich structural and functional modules that form close contact with the surrounding substrate. They play a role in the control of the migration of malignant tumour cells by means of signalling molecules such as PI3K and Rho GTPases for example. We have demonstrated that both MDA-MB-231 and MDA-MB-435s cell migration are inhibited by silencing of gelsolin (Supplemental data Figure 2D). We suggest that gelsolin may contribute to breast cancer cell migration through modification of the actin cytoskeleton, and TRPV2 may also control the remodelling of the actin cytoskeleton required for cell deformation during the migration/invasion process. Recent studies have shown that gelsolin is associated with advanced stage or poor prognosis in uterine cervical cancer [52], non-small cell lung cancer [53], breast cancer [54] and urothelial cancer [55]. PI3K/Akt signalling is critical for the development, progression, and metastasis of malignant tumours. Our results showed a direct effect of TRPV2 on Akt phosphorylation. Recently, girdin, an actin-binding protein, has been ascribed a function in Akt signalling. This protein is known to be phosphorylated by Akt on S1416 residue in some, but not all, cases of breast cancer, colon cancer, and glioblastoma [40, 56, 57]. Girdin plays a crucial role in breast cancer invasion and metastasis and is highly expressed in a portion of many forms of human colon, breast, and cervical carcinomas [58]. Our study showed that girdin can modulate the

TRPV2 dependant breast cancer cell migration (Supplemental data Figure 2C). Moreover, our result demonstrated that TRPV2 can modulate the phosphorylation of girdin on the S1416 residue. Girdin may be involved in various cellular processes, including signalling from G protein-coupled receptors or membrane trafficking, such as endocytosis and exocytosis. Several lines of evidence suggest the presence of endocytosis at the leading edge of migrating cells and its roles in promoting cell migration by participating in lamellipodia extension [59]. Thus, a comprehensive picture of girdin's interactions with the TRPV2 channels and cytoskeleton is still to be defined. Another limitation is that most are *in vitro* experiments that do not address the potential upstream regulator(s) of the tumour microenvironment, such as soluble growth factors, cytokines, and chemokines that may induce girdin's phosphorylation in breast cancer cell lines. This could explain that cell migration is less decreased using a pharmacologic Akt inhibitor, rather than a siRNA strategy, against girdin (Figure 2B, D).

TRPV2 modulated P-Akt and thus regulated the activation of girdin. Our data suggest that the activation of PI3K/Akt could modulate the small G protein Rac1 during the process of controlling TRPV2-dependent cell migration. TRPV2 function could be rapidly regulated by post-translational modifications such as PKA- or PI3K-dependent phosphorylation/dephosphorylation. Correspondingly, TRPV2 has been involved in a signaling module in mast cells that comprises PKA and a protein with a kinase adapter protein-like properties [60]. TRPV2 may be regulated by lysophospholipids and is known to stimulate cancer cell migration [23, 61, 62]. Alkyl ether phospholipids represent an important group of phospholipids characterized by an alkyl or an alkenyl bond at the sn-1 position of the glycerol backbone, and it is generally accepted that endogenous alkyl-ether-lipids are more abundant in tumours than in normal tissue [27]. Here, we focused on the effect of a synthetic alkyl-ether-lipid, AD-HGPC, on TRPV2-dependent cell migration. It is reasonable to suppose that the incorporation of AD-HGPC into the membrane of cells alters the supramolecular packing of lipids and, consequently, the mechanical properties of the membrane as previously observed [63], thus affecting Ca^{2+} channel function. The ion channel function at the surface of the cell can be up- or down-regulated by modulating the number of channels expressed on the surface of the plasma membrane. This regulation may involve translocation of new channels via Golgi stimulation. We found that AD-HGPC induced the translocation of TRPV2 protein to the plasma membrane by Golgi stimulation through the PI3K/Akt/Rac1 pathway. The translocation and activity of TRPV2 is more efficient with the synthetic alkyl-ether-lipid AD-HGPC in comparison with LPC. This effect is may be due to a different kinetic effect and specificity between AD-HGPC and LPC. Indeed, in Figure 5C, AD-HGPC has a slower but

stronger effect on TRPV2 current compared to LPC. AD-HGPC increases TRPV2-dependent cell migration *in vitro* by stimulation of the PI3K/AKT/Rac1 pathway. This stimulation could lead to an enhanced exocytotic response, which could increase the quantity of TRPV2 at the plasma membrane and CCE. Whereas AD-HGPC increases TRPV2-dependent cell migration *in vitro*, we did not observe any effect on the *in vivo* development of metastases, but we did observe an increase in tumour volume. The *in-vitro* and *in-vivo* difference may be explained by the metabolic fate of AD-HGPC. Autotaxin (ATX) has lysophospholipase D activity which leads to tumor cell growth and motility through the production of lysophosphatidic acid [64]. The authors showed that ATX mediates the production of LPA from LPC, ATX could show proliferation-stimulating activity, especially in the presence of exogenous LPC. They demonstrated that recombinant ATX stimulates the proliferation of breast cancer cell line MDA-MB-231. The proliferation-stimulating activity of ATX was significantly enhanced by the supplementation of LPC in extracellular media. In this case the ATX could modify the structure of our compound in vivo leading to a new derivative not as specific as the first one. This effect may be due to the concentration used *in vivo* (0.1 mg/kg) not being enough efficient enough to see an effect on the development of metastases. It would be interesting to increase the concentration to 10 mg/kg with the same *in vivo* protocol. Other possibilities include the following: i) involvement of the tumour microenvironment, which can modify the access of AD-HGPC to cancer cells and ii) AD-HPC can target areas other than tumours. In this way, a quantification of AD-HPC in both tumour and other tissues of treated mice compared to untreated should be performed. It has been demonstrated that a synthetic alkyl-lipid edelfosine accumulates preferentially in tumour cells in both *in vitro* [65-67] and *in vivo* studies [68, 69].

In the literature, synthetic lipids are metabolically stable LPC derivatives, encompassing a class of non-mutagenic drugs that selectively target cancer cells. Some alkylphospholipids (e.g. edelfosine: 1-O-octadecyl-2-O-octadecyl-methyl-rac-glycero-3-phosphocholine) selectively induce FAS death receptors-dependent apoptotic death of cancer cells. Edelfosine targets lipid rafts and modifies the signalling cascades of phospholipases D and C, which in turn abrogate the PI3K/Akt/mTOR and RAS/RAF/MEK/ERK pathways [70]. These changes lead to cell accumulation in the G2/M phase and consequent programmed cell death. Thus, apoptosis induced by edelfosine depends on the release of the Bax/Bak-mediated Ca^{2+} stored in the endoplasmic reticulum (ER). AD-HGPC has structural similarities with edelfosine and LPC. We assume that low concentrations (the ones we have used in this article) are not sufficient to stimulate calcium overload and calcium-dependent apoptosis [71]. At this

concentration, we have an increase of migration and CCE, along with activation of the Akt pathway. In the literature, edelfosine at 10 µM can inhibit Akt phosphorylation, mTOR phosphorylation and Raf downward regulation. The dose effect of AD-HGPC, in the same pattern as observed with edelfosine, reduces viability when the compound is used at more than 10 µM. These experiments reveal a dual effect of AD-HGPC: pro-tumoural at low concentration (100 nM–2 µM) and anti-tumoural at high concentration (30–100 µM) (Supplemental Figure 1E). We can also suspect a proportional effect linked to the amount of cytosolic or ER calcium stress. This "high concentration effect" makes synthetic alkylphospholipids attractive as innovative candidates for personalized therapy. Several studies have shown that alkyl-ether-lipids accumulate preferentially in tumour cells in *in vivo* studies [68, 72]. The favourable safety and tolerability profiles of alkyl-ether-lipids, such as perifosine (an edelfosine derivative), together with the widely reported potentiation of the anti-tumour activity following the combination of perifosine with other anti-tumour drugs and radiotherapy in *in vitro* and pre-clinical assays [73, 74], warrant additional well-designed *in vitro* and *in vivo* studies using combination therapy (immunotherapy or chemotherapy) in the future.

More recently, TRPV2 channel expression in TNBC was associated with a better prognosis and its activation *in vivo* by cannabidiol (CBD) enhances the uptake and efficacy of chemotherapy [19]. The application of AD-HGPC alone shows a protumoral effect *in-vivo* and *in vitro* as well as the activation of resistance pathways such as the PI3K/Akt pathway.In view of these elements, it seems interesting to test the association of AD-HGPC with chemotherapy to reveal or not the interest of the association in chemosensitization. Thus, using AD-HGPC as potent activator of TRPV2 activity and/or TRPV2 trafficking to the plasma membrane could be efficient in TNBC to enhance the uptake and efficacy of chemotherapy. Recently, the Binshtok group showed that co-application of CBD or 2-APB (a TRPV2 channel activator) with doxorubicin resulted in a significantly higher accumulation of doxorubicin in hepatocellular carcinoma cell lines compared to the same cell lines exposed to doxorubicin alone. In addition, the authors demonstrated that undereffective doses of doxorubicin applied in combination with 2-APB or CBD resulted in a significant decrease in the number of living colonies of hepatocellular carcinoma cells compared to the application of doxorubicin alone. Taken together, these results showed a sensitization to the cancer cell death caused by doxorubicin in combination with CBD [75]. TRPV2 activation does not seem to be directly linked to tumour burden, but its translocation to the plasma membrane could be used as a therapeutic target in the case of chemosensitization.

Application of TRPV2 as a direct target in cancer therapy is still in its infancy. Tranilast is the most current blocker of TRPV2 channels used in clinical trials. It is an anti-allergy drug approved for use in Japan and South Korea, and it is also used against asthma, autoimmune diseases, and atopic and fibrotic pathologies. The antitumor potential of tranilast is attracting considerable interest [76]. It was observed that tranilast reduced (> 50%) the growth of primary breast tumours with more than 90% reduction of metastases in a mice model [77]. Nonetheless, one drawback of tranilast is its side effects. The most typical side effect was liver dysfunction, which occurred mainly within 1 month after administration of the drug. Other side effects were seen in the digestive, skin, and urinary systems. However, the recent determination of the three-dimensional structure of TRPV2 and its channel functions [78] and the availability of specific monoclonal antibodies [37] open new prospective and hope for the application of TRPV2-targeted therapy in cancers. In the near future, a distrust must be raised on with regard to TRPV2 as a therapeutic target. TRPV2 has been shown to play important roles in skeletal, cardiac, muscular, immune, and neuronal physiology. Thus, a therapy targeting this receptor must be taken into consideration, as well as its potential side effects. Altogether, our data suggest that activation of TRPV2 by alkyl-ether-lipids or the inhibition of its activity can be used for research in the treatment of metastatic cancer to directly target the primary tumour or to potentiate a chemotherapeutic agent.

6. Conclusion

In conclusion, the alkyl ether lipid-sensitive channel TRPV2, which is highly expressed in high-grade breast tumour tissues, promotes CCE and breast cancer cell migration through the PI3K/Akt-girdin axis. Synthetic alkyl-ether-lipids address the TRPV2 channel through Golgi stimulation and PI3K/Akt/Rac-dependent cytoskeletal reorganization, promoting CCE. We highlight, for the first time, the potential modulation of TRPV2 trafficking by alkyl-ether-lipids as a novel avenue for research in the treatment of metastatic cancer.

References

1. Caterina MJ, Rosen TA, Tominaga M, Brake AJ, Julius D. (1999) A capsaicin-receptor homologue with a high threshold for noxious heat. Nature, 398, 436-41.
2. Mercado J, Gordon-Shaag A, Zagotta WN, Gordon SE. (2010) Ca2+-dependent desensitization of TRPV2 channels is mediated by hydrolysis of phosphatidylinositol 4,5-bisphosphate. J Neurosci, 30, 13338-47.
3. Holakovska B, Grycova L, Bily J, Teisinger J. (2011) Characterization of calmodulin binding domains in TRPV2 and TRPV5 C-tails. Amino Acids, 40, 741-8.

4. Jahnel R, Bender O, Munter LM, Dreger M, Gillen C, Hucho F. (2003) Dual expression of mouse and rat VRL-1 in the dorsal root ganglion derived cell line F-11 and biochemical analysis of VRL-1 after heterologous expression. Eur J Biochem, 270, 4264-71.
5. Nedungadi TP, Dutta M, Bathina CS, Caterina MJ, Cunningham JT. (2012) Expression and distribution of TRPV2 in rat brain. Exp Neurol, 237, 223-37.
6. Park U, Vastani N, Guan Y, Raja SN, Koltzenburg M, Caterina MJ. (2011) TRP vanilloid 2 knock-out mice are susceptible to perinatal lethality but display normal thermal and mechanical nociception. J Neurosci, 31, 11425-36.
7. Rubinstein J, Lasko VM, Koch SE, Singh VP, Carreira V, Robbins N, Patel AR, Jiang M, Bidwell P, Kranias EG, Jones WK, Lorenz JN. (2014) Novel role of transient receptor potential vanilloid 2 in the regulation of cardiac performance. Am J Physiol Heart Circ Physiol, 306, H574-84.
8. Hisanaga E, Nagasawa M, Ueki K, Kulkarni RN, Mori M, Kojima I. (2009) Regulation of calcium-permeable TRPV2 channel by insulin in pancreatic beta-cells. Diabetes, 58, 174-84.
9. Saunders CI, Kunde DA, Crawford A, Geraghty DP. (2007) Expression of transient receptor potential vanilloid 1 (TRPV1) and 2 (TRPV2) in human peripheral blood. Mol Immunol, 44, 1429-35.
10. Stokes AJ, Wakano C, Del Carmen KA, Koblan-Huberson M, Turner H. (2005) Formation of a physiological complex between TRPV2 and RGA protein promotes cell surface expression of TRPV2. J Cell Biochem, 94, 669-83.
11. Zhang D, Spielmann A, Wang L, Ding G, Huang F, Gu Q, Schwarz W. (2012) Mast-cell degranulation induced by physical stimuli involves the activation of transient-receptor-potential channel TRPV2. Physiol Res, 61, 113-24.
12. Kato K, Morita I. (2013) Promotion of osteoclast differentiation and activation in spite of impeded osteoblast-lineage differentiation under acidosis: effects of acidosis on bone metabolism. Biosci Trends, 7, 33-41.
13. Nabissi M, Morelli MB, Amantini C, Farfariello V, Ricci-Vitiani L, Caprodossi S, Arcella A, Santoni M, Giangaspero F, De Maria R, Santoni G. (2010) TRPV2 channel negatively controls glioma cell proliferation and resistance to Fas-induced apoptosis in ERK-dependent manner. Carcinogenesis, 31, 794-803.
14. Santoni G, Amantini C, Maggi F, Marinelli O, Santoni M, Nabissi M, Morelli MB. (2019) The TRPV2 cation channels: from urothelial cancer invasiveness to glioblastoma multiforme interactome signature. Lab Invest.
15. Caprodossi S, Lucciarini R, Amantini C, Nabissi M, Canesin G, Ballarini P, Di Spilimbergo A, Cardarelli MA, Servi L, Mammana G, Santoni G. (2008) Transient receptor potential vanilloid type 2 (TRPV2) expression in normal urothelium and in urothelial carcinoma of human bladder: correlation with the pathologic stage. Eur Urol, 54, 612-20.
16. Yamada T, Ueda T, Shibata Y, Ikegami Y, Saito M, Ishida Y, Ugawa S, Kohri K, Shimada S. (2010) TRPV2 activation induces apoptotic cell death in human T24 bladder cancer cells: a potential therapeutic target for bladder cancer. Urology, 76, 509 e1-7.
17. Liu Q, Wang X. (2013) Effect of TRPV2 cation channels on the proliferation, migration and invasion of 5637 bladder cancer cells. Exp Ther Med, 6, 1277-1282.
18. Oulidi A, Bokhobza A, Gkika D, Vanden Abeele F, Lehen'kyi V, Ouafik L, Mauroy B, Prevarskaya N. (2013) TRPV2 mediates adrenomedullin stimulation of prostate and urothelial cancer cell adhesion, migration and invasion. PLoS One, 8, e64885.
19. Elbaz M, Ahirwar D, Xiaoli Z, Zhou X, Lustberg M, Nasser MW, Shilo K, Ganju RK. (2018) TRPV2 is a novel biomarker and therapeutic target in triple negative breast cancer. Oncotarget, 9, 33459-33470.
20. De Petrocellis L, Ligresti A, Moriello AS, Allara M, Bisogno T, Petrosino S, Stott CG, Di Marzo V. (2011) Effects of cannabinoids and cannabinoid-enriched Cannabis extracts on TRP channels and endocannabinoid metabolic enzymes. Br J Pharmacol, 163, 1479-94.

21. Bang S, Kim KY, Yoo S, Lee SH, Hwang SW. (2007) Transient receptor potential V2 expressed in sensory neurons is activated by probenecid. Neurosci Lett, 425, 120-5.
22. Nie L, Oishi Y, Doi I, Shibata H, Kojima I. (1997) Inhibition of proliferation of MCF-7 breast cancer cells by a blocker of Ca(2+)-permeable channel. Cell Calcium, 22, 75-82.
23. Monet M, Gkika D, Lehen'kyi V, Pourtier A, Vanden Abeele F, Bidaux G, Juvin V, Rassendren F, Humez S, Prevarsakaya N. (2009) Lysophospholipids stimulate prostate cancer cell migration via TRPV2 channel activation. Biochim Biophys Acta, 1793, 528-39.
24. Cao E, Cordero-Morales JF, Liu B, Qin F, Julius D. (2013) TRPV1 channels are intrinsically heat sensitive and negatively regulated by phosphoinositide lipids. Neuron, 77, 667-79.
25. Girault A, Haelters JP, Potier-Cartereau M, Chantome A, Pinault M, Marionneau-Lambot S, Oullier T, Simon G, Couthon-Gourves H, Jaffres PA, Corbel B, Bougnoux P, Joulin V, Vandier C. (2011) New alkyl-lipid blockers of SK3 channels reduce cancer cell migration and occurrence of metastasis. Curr Cancer Drug Targets, 11, 1111-25.
26. Potier M, Chantome A, Joulin V, Girault A, Roger S, Besson P, Jourdan ML, LeGuennec JY, Bougnoux P, Vandier C. (2011) The SK3/K(Ca)2.3 potassium channel is a new cellular target for edelfosine. Br J Pharmacol, 162, 464-79.
27. Snyder F, Wood R. (1969) Alkyl and alk-1-enyl ethers of glycerol in lipids from normal and neoplastic human tissues. Cancer Res, 29, 251-7.
28. Brohult A, Brohult J, Brohult S. (1978) Regression of tumour growth after administration of alkoxyglycerols. Acta Obstet Gynecol Scand, 57, 79-83.
29. Pedrono F, Martin B, Leduc C, Le Lan J, Saiag B, Legrand P, Moulinoux JP, Legrand AB. (2004) Natural alkylglycerols restrain growth and metastasis of grafted tumors in mice. Nutr Cancer, 48, 64-9.
30. Brohult A, Brohult J, Brohult S, Joelsson I. (1977) Effect of alkoxyglycerols on the frequency of injuries following radiation therapy for carcinoma of the uterine cervix. Acta Obstet Gynecol Scand, 56, 441-8.
31. Chantome A, Potier-Cartereau M, Clarysse L, Fromont G, Marionneau-Lambot S, Gueguinou M, Pages JC, Collin C, Oullier T, Girault A, Arbion F, Haelters JP, Jaffres PA, Pinault M, Besson P, Joulin V, Bougnoux P, Vandier C. (2013) Pivotal role of the lipid Raft SK3-Orai1 complex in human cancer cell migration and bone metastases. Cancer Res, 73, 4852-61.
32. Chandrakumar NS HJ. (1983) Stereospecific Synthesis of Ether Phospholipids. Preparation of1- Alkyl-2-(acylamino)-2-deoxyglycerophosphorylhco lines. J. Org. Chem, 1197-1202.
33. Ponpipom M.M BRL. (1984) SYNTHESIS OF AZIDE AND AMIDE ANALOGS OF PLATELET-ACTIVATINGFACTOR AND RELATED DERIVATIVES. Chem. Phys. Lipids, 35, 29-37.
34. Chantome A, Girault A, Potier M, Collin C, Vaudin P, Pages JC, Vandier C, Joulin V. (2009) KCa2.3 channel-dependent hyperpolarization increases melanoma cell motility. Exp Cell Res, 315, 3620-30.
35. Potier M, Joulin V, Roger S, Besson P, Jourdan ML, Leguennec JY, Bougnoux P, Vandier C. (2006) Identification of SK3 channel as a new mediator of breast cancer cell migration. Mol Cancer Ther, 5, 2946-53.
36. Brouard T CA. (2009) Automatic nuceli cell counting in low-resolution fluorescence imagesComputational Vision and Medical Image Processing83-8.
37. Chubb D, Weinhold N, Broderick P, Chen B, Johnson DC, Forsti A, Vijayakrishnan J, Migliorini G, Dobbins SE, Holroyd A, Hose D, Walker BA, Davies FE, Gregory WA, Jackson GH, Irving JA, Pratt G, Fegan C, Fenton JA, Neben K, Hoffmann P, Nothen MM, Muhleisen TW, Eisele L, Ross FM, Straka C, Einsele H, Langer C, Dorner E, Allan JM, Jauch A, Morgan GJ, Hemminki K, Houlston RS, Goldschmidt H. (2013) Common variation at 3q26.2, 6p21.33, 17p11.2 and 22q13.1 influences multiple myeloma risk. Nat Genet, 45, 1221-5.
38. Sander EE, van Delft S, ten Klooster JP, Reid T, van der Kammen RA, Michiels F, Collard JG. (1998) Matrix-dependent Tiam1/Rac signaling in epithelial cells promotes either cell-cell

adhesion or cell migration and is regulated by phosphatidylinositol 3-kinase. J Cell Biol, 143, 1385-98.

39. Wang H, Zhang J, Zhang M, Wei L, Chen H, Li Z. (2017) A systematic study of Girdin on cell proliferation, migration and angiogenesis in different breast cancer subtypes. Mol Med Rep, 16, 3351-3356.
40. Yamamura Y, Asai N, Enomoto A, Kato T, Mii S, Kondo Y, Ushida K, Niimi K, Tsunoda N, Nagino M, Ichihara S, Furukawa K, Maeda K, Murohara T, Takahashi M. (2015) Akt-Girdin signaling in cancer-associated fibroblasts contributes to tumor progression. Cancer Res, 75, 813-23.
41. Prevarskaya N, Zhang L, Barritt G. (2007) TRP channels in cancer. Biochim Biophys Acta, 1772, 937-46.
42. Santoni G, Farfariello V. (2011) TRP channels and cancer: new targets for diagnosis and chemotherapy. Endocr Metab Immune Disord Drug Targets, 11, 54-67.
43. Gkika D, Prevarskaya N. (2011) TRP channels in prostate cancer: the good, the bad and the ugly? Asian J Androl, 13, 673-6.
44. Prevarskaya N, Flourakis M, Bidaux G, Thebault S, Skryma R. (2007) Differential role of TRP channels in prostate cancer. Biochem Soc Trans, 35, 133-5.
45. Ziglioli F, Frattini A, Maestroni U, Dinale F, Ciufifeda M, Cortellini P. (2009) Vanilloid-mediated apoptosis in prostate cancer cells through a TRPV-1 dependent and a TRPV-1-independent mechanism. Acta Biomed, 80, 13-20.
46. Monet M, Lehen'kyi V, Gackiere F, Firlej V, Vandenberghe M, Roudbaraki M, Gkika D, Pourtier A, Bidaux G, Slomianny C, Delcourt P, Rassendren F, Bergerat JP, Ceraline J, Cabon F, Humez S, Prevarskaya N. (2010) Role of cationic channel TRPV2 in promoting prostate cancer migration and progression to androgen resistance. Cancer Res, 70, 1225-35.
47. Dvorak MM, Riccardi D. (2004) Ca2+ as an extracellular signal in bone. Cell Calcium, 35, 249-55.
48. McGough AM, Staiger CJ, Min JK, Simonetti KD. (2003) The gelsolin family of actin regulatory proteins: modular structures, versatile functions. FEBS Lett, 552, 75-81.
49. Chellaiah M, Kizer N, Silva M, Alvarez U, Kwiatkowski D, Hruska KA. (2000) Gelsolin deficiency blocks podosome assembly and produces increased bone mass and strength. J Cell Biol, 148, 665-78.
50. Chellaiah MA. (2006) Regulation of podosomes by integrin alphavbeta3 and Rho GTPase-facilitated phosphoinositide signaling. Eur J Cell Biol, 85, 311-7.
51. Nagasawa M, Kojima I. (2012) Translocation of calcium-permeable TRPV2 channel to the podosome: Its role in the regulation of podosome assembly. Cell Calcium, 51, 186-93.
52. Liao CJ, Wu TI, Huang YH, Chang TC, Wang CS, Tsai MM, Hsu CY, Tsai MH, Lai CH, Lin KH. (2011) Overexpression of gelsolin in human cervical carcinoma and its clinicopathological significance. Gynecol Oncol, 120, 135-44.
53. Shieh DB, Godleski J, Herndon JE, 2nd, Azuma T, Mercer H, Sugarbaker DJ, Kwiatkowski DJ. (1999) Cell motility as a prognostic factor in Stage I nonsmall cell lung carcinoma: the role of gelsolin expression. Cancer, 85, 47-57.
54. Thor AD, Edgerton SM, Liu S, Moore DH, 2nd, Kwiatkowski DJ. (2001) Gelsolin as a negative prognostic factor and effector of motility in erbB-2-positive epidermal growth factor receptor-positive breast cancers. Clin Cancer Res, 7, 2415-24.
55. Rao J, Seligson D, Visapaa H, Horvath S, Eeva M, Michel K, Pantuck A, Belldegrun A, Palotie A. (2002) Tissue microarray analysis of cytoskeletal actin-associated biomarkers gelsolin and E-cadherin in urothelial carcinoma. Cancer, 95, 1247-57.
56. Nishimae K, Tsunoda N, Yokoyama Y, Kokuryo T, Iwakoshi A, Takahashi M, Nagino M. (2013) The impact of Girdin expression on recurrence-free survival in patients with luminal-type breast cancer. Breast Cancer.

57. Natsume A, Kato T, Kinjo S, Enomoto A, Toda H, Shimato S, Ohka F, Motomura K, Kondo Y, Miyata T, Takahashi M, Wakabayashi T. (2012) Girdin maintains the stemness of glioblastoma stem cells. Oncogene, 31, 2715-24.
58. Jiang P, Enomoto A, Jijiwa M, Kato T, Hasegawa T, Ishida M, Sato T, Asai N, Murakumo Y, Takahashi M. (2008) An actin-binding protein Girdin regulates the motility of breast cancer cells. Cancer Res, 68, 1310-8.
59. Kruchten AE, McNiven MA. (2006) Dynamin as a mover and pincher during cell migration and invasion. J Cell Sci, 119, 1683-90.
60. Stokes AJ, Shimoda LM, Koblan-Huberson M, Adra CN, Turner H. (2004) A TRPV2-PKA signaling module for transduction of physical stimuli in mast cells. J Exp Med, 200, 137-47.
61. Park KS, Lee HY, Lee SY, Kim MK, Kim SD, Kim JM, Yun J, Im DS, Bae YS. (2007) Lysophosphatidylethanolamine stimulates chemotactic migration and cellular invasion in SK-OV3 human ovarian cancer cells: involvement of pertussis toxin-sensitive G-protein coupled receptor. FEBS Lett, 581, 4411-6.
62. Pebay A, Bonder CS, Pitson SM. (2007) Stem cell regulation by lysophospholipids. Prostaglandins Other Lipid Mediat, 84, 83-97.
63. Herrera FE, Sevrain CM, Jaffres PA, Couthon H, Grelard A, Dufourc EJ, Chantome A, Potier-Cartereau M, Vandier C, Bouchet AM. (2017) Singular Interaction between an Antimetastatic Agent and the Lipid Bilayer: The Ohmline Case. ACS Omega, 2, 6361-6370.
64. Umezu-Goto M, Kishi Y, Taira A, Hama K, Dohmae N, Takio K, Yamori T, Mills GB, Inoue K, Aoki J, Arai H. (2002) Autotaxin has lysophospholipase D activity leading to tumor cell growth and motility by lysophosphatidic acid production. J Cell Biol, 158, 227-33.
65. Gajate C, Del Canto-Janez E, Acuna AU, Amat-Guerri F, Geijo E, Santos-Beneit AM, Veldman RJ, Mollinedo F. (2004) Intracellular triggering of Fas aggregation and recruitment of apoptotic molecules into Fas-enriched rafts in selective tumor cell apoptosis. J Exp Med, 200, 353-65.
66. Gajate C, Mollinedo F. (2007) Edelfosine and perifosine induce selective apoptosis in multiple myeloma by recruitment of death receptors and downstream signaling molecules into lipid rafts. Blood, 109, 711-9.
67. Mollinedo F, Fernandez-Luna JL, Gajate C, Martin-Martin B, Benito A, Martinez-Dalmau R, Modolell M. (1997) Selective induction of apoptosis in cancer cells by the ether lipid ET-18-OCH3 (Edelfosine): molecular structure requirements, cellular uptake, and protection by Bcl-2 and Bcl-X(L). Cancer Res, 57, 1320-8.
68. Estella-Hermoso de Mendoza A, Campanero MA, de la Iglesia-Vicente J, Gajate C, Mollinedo F, Blanco-Prieto MJ. (2009) Antitumor alkyl ether lipid edelfosine: tissue distribution and pharmacokinetic behavior in healthy and tumor-bearing immunosuppressed mice. Clin Cancer Res, 15, 858-64.
69. Mollinedo F, de la Iglesia-Vicente J, Gajate C, Estella-Hermoso de Mendoza A, Villa-Pulgarin JA, Campanero MA, Blanco-Prieto MJ. (2010) Lipid raft-targeted therapy in multiple myeloma. Oncogene, 29, 3748-57.
70. Kaleagasioglu F, Zaharieva MM, Konstantinov SM, Berger MR. (2019) Alkylphospholipids are Signal Transduction Modulators with Potential for Anticancer Therapy. Anticancer Agents Med Chem, 19, 66-91.
71. Nieto-Miguel T, Fonteriz RI, Vay L, Gajate C, Lopez-Hernandez S, Mollinedo F. (2007) Endoplasmic reticulum stress in the proapoptotic action of edelfosine in solid tumor cells. Cancer Res, 67, 10368-78.
72. Mollinedo F, de la Iglesia-Vicente J, Gajate C, Estella-Hermoso de Mendoza A, Villa-Pulgarin JA, de Frias M, Roue G, Gil J, Colomer D, Campanero MA, Blanco-Prieto MJ. (2010) In vitro and In vivo selective antitumor activity of Edelfosine against mantle cell lymphoma and chronic lymphocytic leukemia involving lipid rafts. Clin Cancer Res, 16, 2046-54.

73. Pachioni Jde A, Magalhaes JG, Lima EJ, Bueno Lde M, Barbosa JF, de Sa MM, Rangel-Yagui CO. (2013) Alkylphospholipids - a promising class of chemotherapeutic agents with a broad pharmacological spectrum. J Pharm Pharm Sci, 16, 742-59.
74. Verheij M, Moolenaar WH, Blitterswijk WJ. (2014) Combining anti-tumor alkyl-phospholipid analogs and radiotherapy: rationale and clinical outlook. Anticancer Agents Med Chem, 14, 618-28.
75. Neumann-Raizel H, Shilo A, Lev S, Mogilevsky M, Katz B, Shneor D, Shaul YD, Leffler A, Gabizon A, Karni R, Honigman A, Binshtok AM. (2019) 2-APB and CBD-Mediated Targeting of Charged Cytotoxic Compounds Into Tumor Cells Suggests the Involvement of TRPV2 Channels. Front Pharmacol, 10, 1198.
76. Rogosnitzky M, Danks R, Kardash E. (2012) Therapeutic potential of tranilast, an anti-allergy drug, in proliferative disorders. Anticancer Res, 32, 2471-8.
77. Chakrabarti R, Subramaniam V, Abdalla S, Jothy S, Prud'homme GJ. (2009) Tranilast inhibits the growth and metastasis of mammary carcinoma. Anticancer Drugs, 20, 334-45.
78. Huynh KW, Cohen MR, Chakrapani S, Holdaway HA, Stewart PL, Moiseenkova-Bell VY. (2011) Structural insight into the assembly of TRPV channels. Structure, 22, 260-8.

Author contributions

Maxime Guéguinou, Christophe Vandier and Marie Potier-Cartereau provided the conception and design of the work and wrote the manuscript with contributions from other authors. Maxime Guéguinou, Aubin Penna, Audrey Gambade, Romain Felix, Yann Fourbon, Christophe Arnoult, Thomas Harnois, Aurélie Chantôme, and Ana Bouchet performed experiments and/or data analyses. Günther Weber, Philippe Bougnoux, and Olivier Mignen provided the critical revision of the manuscript. Gaëlle Simon, Jean-Pierre Haelters, and Paul-Alain Jaffrès synthesized the ether alkyl lipid AD-HGPC. François Carreaux synthesized the tranilast. Thibault Oullier and Séverine Marionneau-Lambot performed the *in vivo* experiments. Marie Potier-Cartereau supervised the work.

Conflicts of interest: The authors declare no conflicts of interest.

Funding

This work was funded by INCa, Ligue Nationale Contre le Cancer, Region Centre Val de Loire (LIPIDS project of ARD2020-Biomédicaments), INSERM, Cancéropôle Grand Ouest, the association “CANCEN” and Tours Hospital oncology association “ACORT". M. Gueguinou, Y. Fourbon and A. Gambade held fellowships from the “Region Centre”, “Ministère de l'Enseignement Supérieur et de la Recherche”.

Acknowledgments

The authors thank A. Douaud-Lecaille and I. Domingo for technical assistance and C. Leroy for secretarial support.

Appendix A. Supplementary data

Figures and Legends

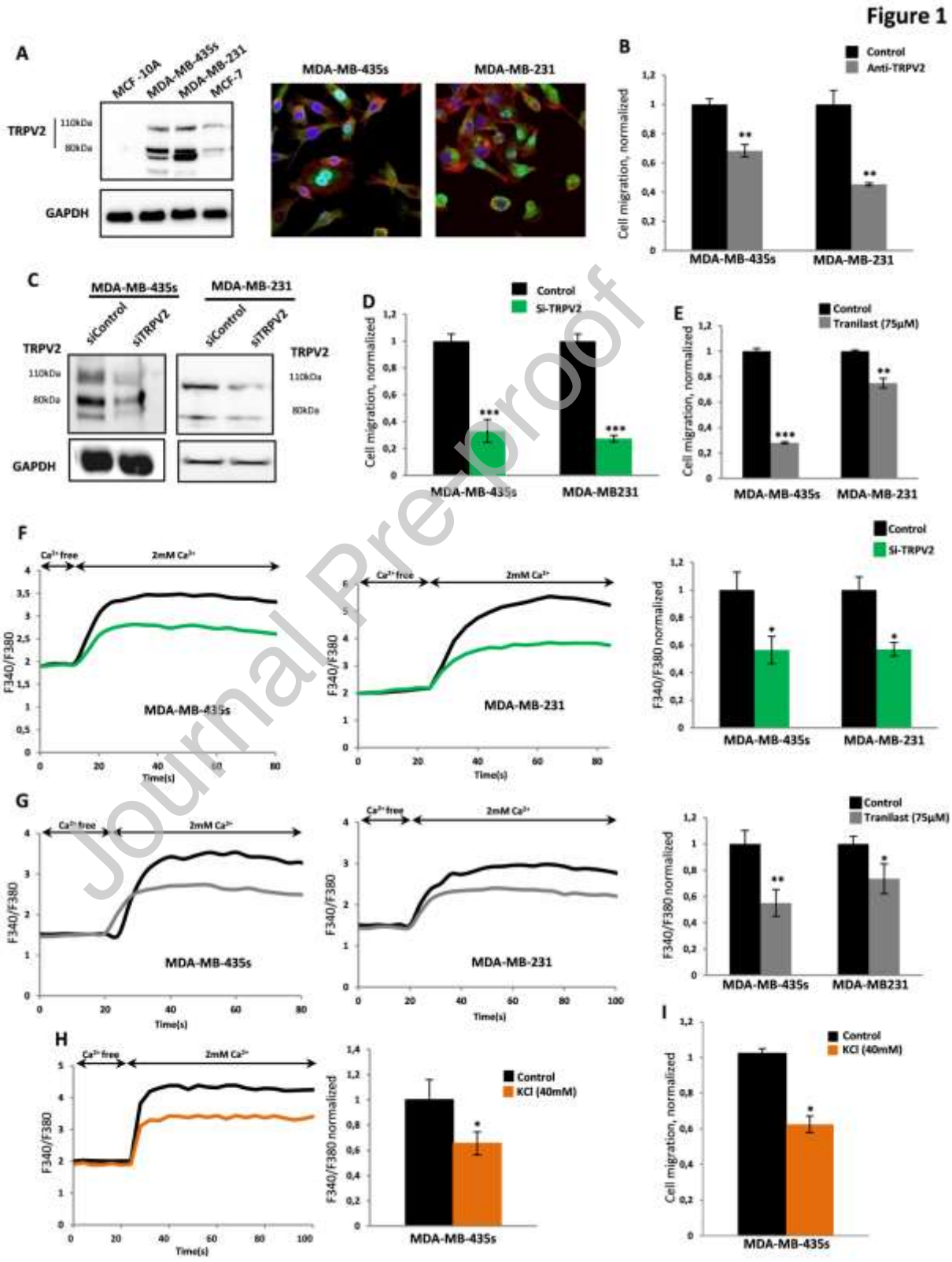

Figure 1: Migration of breast cancer cells is dependent on the TRPV2 channel. **A.** Left, Immunoblots represent TRPV2 expression in breast cancer cells line compared to normal epithelial breast cell line MCF-10A. Right, Expression of TRPV2 channels in MDA-MB-435s and MDA-MB-231 cells was performed by fluorescent staining of TRPV2 channels (green) and F-actin (red). **B.** The TRPV2 channel is involved in breast cancer cell migration. Histograms show MDA-MB-231 (N=3, n=6) or MDA-MB-435s (N=4, n=8) cell migration treated for 24 h with an extracellular antibody directed against TRPV2 *(**$p < 0.01$)*. **C**. TRPV2 extinction was verified by Western blotting after transfection (48 h) in MDA-MB-435s and MDA-MB-231 cells. **D**. and E. The TRPV2 channel is involved in breast cancer cell migration. D. Histograms represent the migration, for 24 h, of MDA-MB-231 *(N=3)* or MDA-MB-435s *(N=5)* cells transfected with siTRPV2 for 48 h (mean +/- SEM, ***$p < 0.001$). **E**. Histograms show MDA-MB-231 or MDA-MB-435s cell migration treated for 24 h with tranilast (75 µM) *(N=3, n=6)* or an extracellular antibody against TRPV2 *(N=5, n=10)* (mean+/- SEM, ***$p < 0.001$, **$p < 0.01$). **F**. The TRPV2 channel promoted constitutive Ca^{2+} entry in breast cancer cell lines. Fluorescence measurement and relative fluorescence to Ca^{2+}entry in MDA-MB-435s and MDA-MB-231 cells transfected or not with siRNA directed against TRPV2Data were normalized to control conditions. *(mean +/- SEM, N=5,*$p < 0.05$)*. **G**. Fluorescence measurement and relative fluorescence to Ca^{2+}entry in MDA-MB-435s and MDA-MB-231cells treated with tranilast (75 µM) and DMSO (control). Histograms show mean +/- SEM of ratiometric fluorescence in MDA-MB-435s *(N=7)* and MDA-MB-231*(N=8)* cells treated with tranilast *vs* control. Data were normalized to control condition (**$p <$ 0.01; *$p < 0.05$). **H**. Fluorescence measurement and relative fluorescence to Ca^{2+}entry in MDA-MB-435s cells cultured in medium with 40 mM KCl and 40 mM NaCl (control condition). Histograms show mean +/- SEM of ratiometric fluorescence. Data were normalized to control conditions (N=5, *$p < 0.05$). **I.** Depolarization induced by 40 mM KCl decreased breast cancer cell migration. Histograms show MDA-MB-435s cell migration treated with 40 mM KCl for 24 h compared to control *(mean +/- SEM , N=3, n=6* *$p < 0.05$).

Figure 2

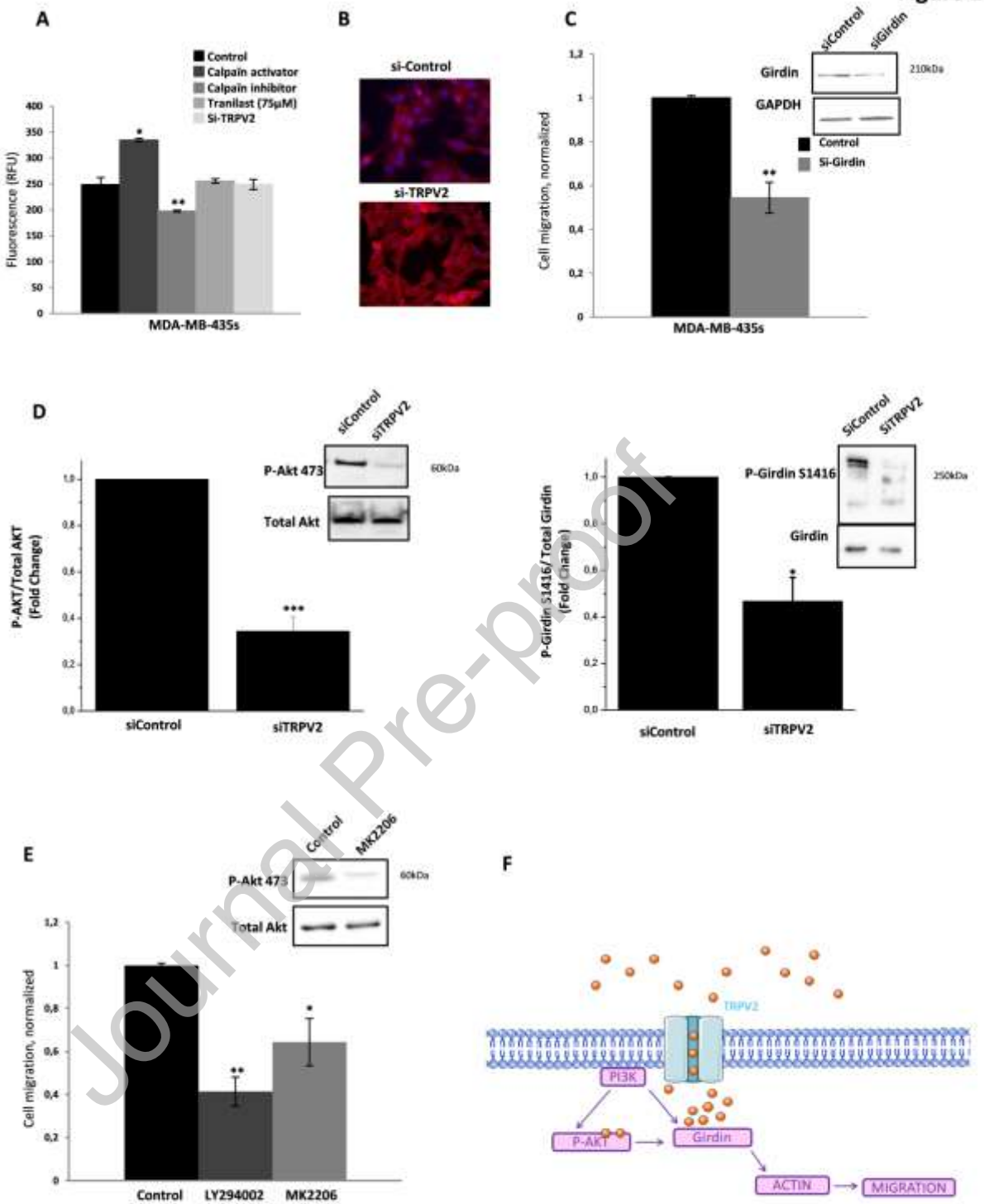

Figure 2: Calcium influx and the Akt signalling pathway regulate breast cancer cell motility. **A**. Treatment with tranilast (75 µM) or TRPV2 knock-down have no effect on calpain activity (N=3, n=6). **B**. TRPV2 extinction by siRNA, in MDA-MB-435s cells, seems to affect cytoskeleton organization. Immunostaining of F-actin by phalloidin-594 was performed in MDA-MB-435s cells. Cells were seeded on fibronectin. **C**. Girdin is involved in breast cancer cell migration. Histograms show MDA-MB-435s cell migration transfected for 48 h with si-girdin *(mean+/- SEM, N=3, n=9, *p < 0.01)*. Inset, girdin extinction was verified by immunoblots after transfection (48 h). **D**. TRPV2 knock-down inhibits Akt (Left) and girdin (Right) phosphorylation. Histograms show the decrease of P-Akt *(N=4)* and P-Girdin *(N=5)* after si-TRPV2 transfection (48 h) of MDA-MB-435s cells *(mean+/- SEM, ***p < 0.001 and *p < 0.05*). **E**. TRPV2-dependent migration of MDA-MB-435s cells is controlled by the PI3K/Akt signalling pathway. Breast cancer cell migration is decreased by LY294002 (inhibitor of PI3K) or MK2206 (inhibitor of Akt). Histograms show migration of MDA-MB-435s cells treated by LY294002 (*N=3, n=6)* or MK2206 (*N=3, n=9)* compared to control condition (mean +/- SEM, ***p < 0.01 and *p < 0.05)*. Inset, immunoblots showing the decrease of P-Akt expression after treatment with MK2206 (1 h). **F**. Hypothetical schema represents TRPV2 channel involvement in PI3K/Akt-dependent breast cancer cell migration associated with girdin in MDA-MB-435s cells.

Figure 3

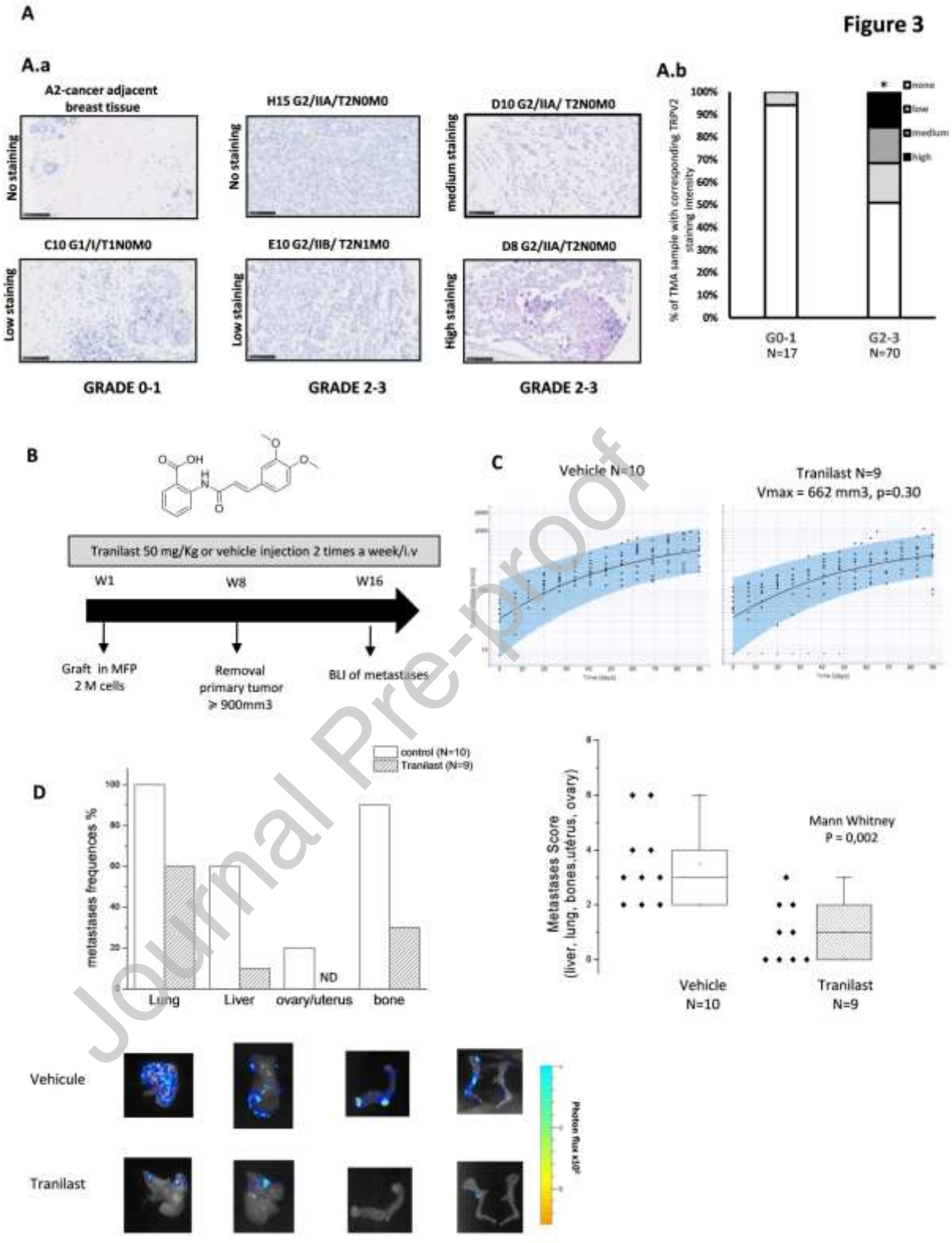

Figure 3: TRPV2 expression is correlated to histologic grade of breast cancer, and its inhibition by tranilast decreases the development of metastases *in vivo*. **A**. Aa. Representative image of immunohistochemical (IHC) staining showing different levels of TRPV2 expression observed in the tissue microarray (TMA) according to the indicated grade/stage. Ab. Quantitation of TRPV2 expression in normal and breast cancer tissues of the TMA used in the study according to pathology grade or clinical stage of breast cancer based on TNM grouping (UICC staging). N indicates the numbers of normal and breast cancer tissues of the TMA used. *(*p < 0.05).* **B**. MFP tumour model protocol used for tranilast injections. **C**. Breast primary tumour volume is not influenced by TRPV2 channels. Graph showing tumour volume across time in MDA-MB-435s grafted mice treated with or without tranilast. Black dots are measured tumour volumes, blue areas are 90% model prediction intervals and line is median tumour growth. **D**. Treatment with tranilast decreases metastases in the MFP tumour model. Frequencies of metastases (lung, bone, liver, and uterus/ovary) in mice treated with either tranilast or vehicle and representative *ex vivo* bioluminescent images of metastases. Box plots indicate the first, median, and third quartiles, while the squares indicate the mean. N indicates the number of mice.

Figure 4

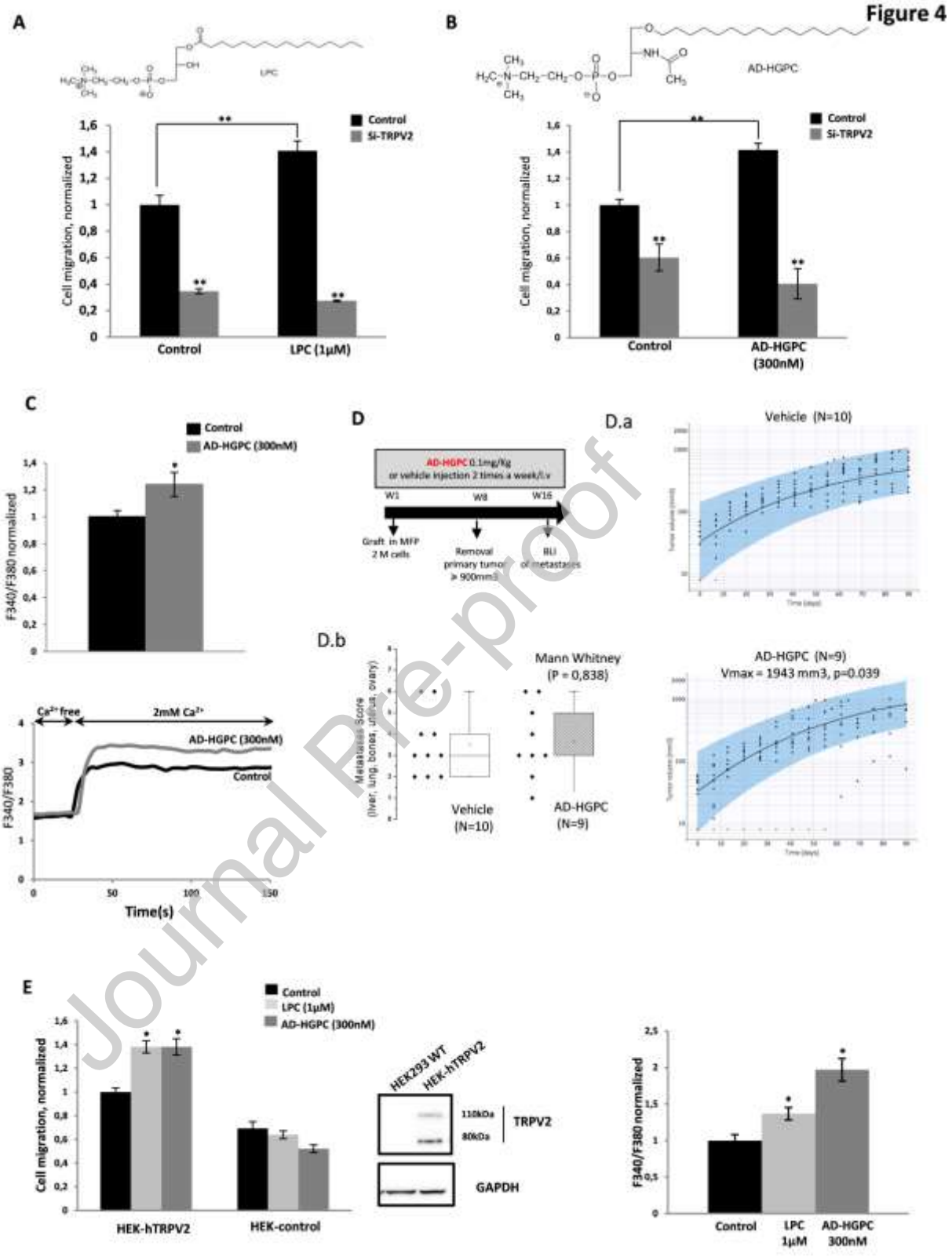

Figure 4: LPC and AD-HGPC increase TRPV2-dependent cell migration without affecting tumour progression and development of metastases. **A, B**. Molecular structures of LPC and AD-HGPC are described in the insets. Stimulation of migration by LPC **(A)** or AD-HGPC (**B**) is dependent on TRPV2 activity. Histograms showing migration (24 h) of MDA-MB-435s cells treated with LPC 1 µM (*N=3, n=6)* or AD-HGPC 300 nM (*N=3, n=9)* +/- siTRPV2 *(mean +/- SEM, **p < 0.01).* **C**. TRPV2 channel promoted constitutive Ca^{2+} entry in MDA-MB-435s cells. Fluorescence measurement and relative fluorescence to Ca^{2+} entry in MDA-MB-435s cells treated with or without AD-HGPC for 24 h. Histograms show mean +/- SEM of ratiometric fluorescence. Data were normalized to control conditions *(N=5, *p < 0.05)*. **D**. MFP tumour model protocol used for AD-HGPC injections. Breast primary tumour volume is influenced by activation of TRPV2 by AD-HGPC. Graph showing tumour volume across time in MDA-MB-435s grafted mice treated with or without AD-HGPC. Black dots are measured tumour volumes, blue areas are 90% model prediction intervals and line is median tumour growth (Da). Occurrence of metastases (lung, bone, liver, and uterus/ovary) in mice treated with either AD-HGPC or vehicle (Db). Box plots indicate the first, median, and third quartiles, while the squares indicate the mean. N indicates the number of mice. **E**. **Left panel**. TRPV2 expression increases HEK293 cell migration. Histograms showing cell migration of HEK-TRPV2 and HEK-control cells treated with or without LPC (1 µM) or AD-HGPC (300 nM) for 24 h *(mean +/- SEM, N=3, n=9, *p < 0.05).* Inset, immunoblots showing TRPV2 expression channel in HEK293 cells compared to HEK293 wild type cells. **E**. **Right panel**. Constitutive calcium entry in HEK-TRPV2 cells is increased by treatment with LPC (1 µM) or AD-HGPC (300 nM). Histograms show of ratiometric fluorescence to Ca^{2+}entry in HEK-TRPV2 cells treated with or without AD-HGPC *(N=3)* or LPC *(N=5)* for 24 h. Data were normalized to conditions obtained with untreated HEK-TRPV2 cells *(*mean +/- SEM , **p < 0.05).*

Figure 5

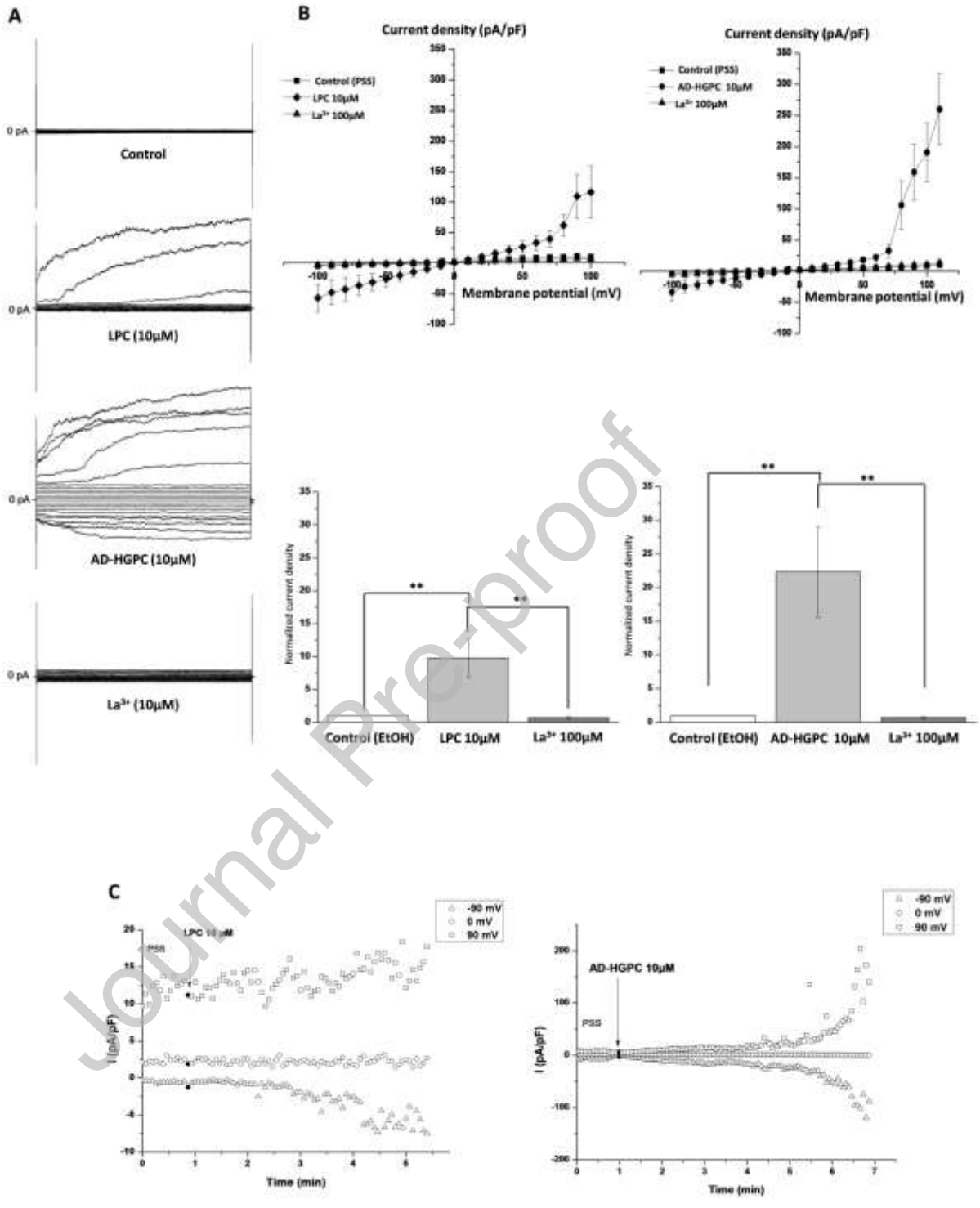

Figure 5: LPC and AD-HGPC increase TRPV2 channel activity. **A.** Representative TRPV2 whole-cell currents recorded in HEK-TRPV2 cells in the control condition or during acute application of LPC (10 µm), AD-HGPC (10 µM) or La^{3+} (10 µM). Recording of TRPV2 current obtained with an I-V protocol, with or without treatments (LPC or AD-HGPC +/- La^{3+}). **B. Upper panel**. TRPV2 current density voltage relationships obtained in the control condition or after acute application of LPC (10 µM) or AD-HGPC (10 µM) +/- La^{3+}. The current density voltage relation was obtained by dividing the averaged steady-state currents elicited from –100 mV to +100 mV by the respective cell capacitance. **Bottom panel**. Histograms show current density normalized to control (Ethanol) *(mean +/- SEM, N=11 for LPC and N=13 for AD-HGPC, **p < 0.01*). Acute application of LPC (10 µM) or AD-HGPC (10 µM) increases current amplitudes of TRPV2 channels. The increase of TRPV2 current amplitude is totally abolished by La^{2+} (10 µM)(N=10). **C.** Current time relationship after acute application of LPC (10 µM) or AD-HGPC (10 µM) on HEK-TRPV2 cells.

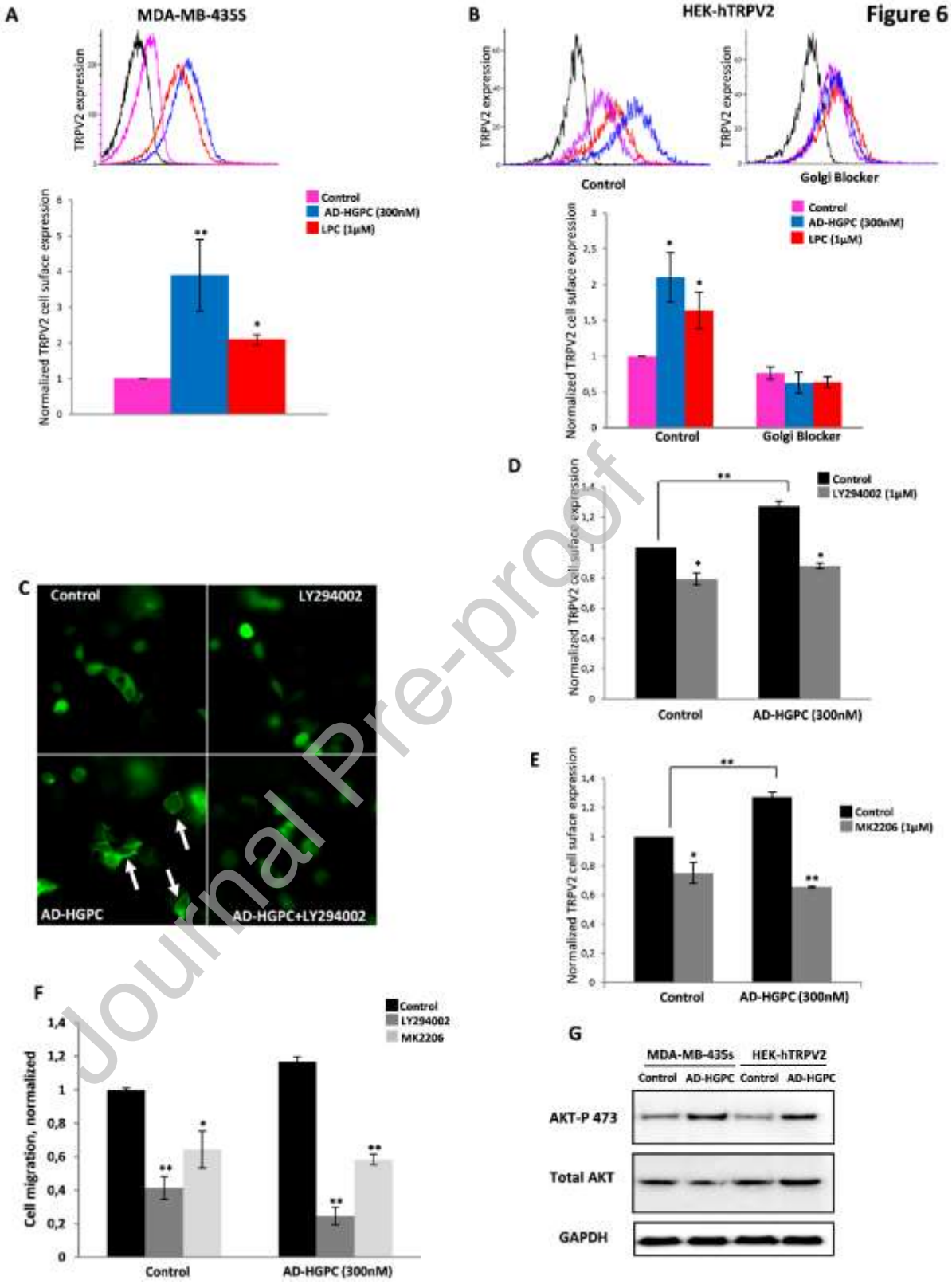

Figure 6: AD-HGPC and LPC induce translocation of TRPV2 to the plasma membrane by the PI3K/Akt pathway. **A**. AD-HGPC and LPC induce translocation of TRPV2 channels to the plasma membrane in MDA-MB-435s cells (Black line represents isotype used as negative control). Histograms show surface expression of TRPV2 in MDA-MB-435s cells after acute application of LPC (1 µM) or AD-HGPC (300 nM) *(mean +/- SEM, N=5, *p < 0.05, **p < 0.01).* **B**. AD-HGPC and LPC induce translocation of TRPV2 channels to the plasma membrane in HEK-TRPV2 cells through Golgi trafficking (Black line represents isotype used as negative control). Histograms show surface expression of TRPV2 in HEK-TRPV2 cells after acute application of LPC or AD-HGPC in presence of Golgi blocker *vs* control (mean+/- SEM, N=4, **p* < 0.05). **C**. AD-HGPC stimulation induces plasma membrane translocation of PI3K. The visualization of PI3K activity is performed by the Btk-PH-GFP fusion protein. Acute stimulation of HEK-TRPV2 cells by AD-HGPC (300 nM) leads to Btk-PH-GFP translocation from the cytoplasm to the plasma membrane. LY294002 (1 µM) pre-treatment decreases the translocation of PI3K in HEK-hTRPV2 cells. **D**. Inhibition of PI3K blocks the translocation of TRPV2 to the plasma membrane of MDA-MB-435s cells. Histograms show the TRPV2 plasma membrane translocation induced by acute application of AD-HGPC is abolished by pre-treatment with LY294002 *(mean +/- SEM, N=3 (control) and N=5 (AD-HGC),*p < 0.05, **p< 0.01*). **E**. The increase of recruitment of TRPV2 is inhibited by pharmacological inhibition of the Akt signalling pathway by MK2206 (1 µM) on MDA-MB-435s cells (mean+/- SEM, N=3 (control) and N=5 *(AD-HGPC), (*p<0.05, **p < 0.01)).* **F**. Increase of MDA-MB-435s cell migration by AD-HGPC is inhibited by LY294002 or MK2206. Histograms show migration of MDA-MB-435s cells treated by PI3K or Akt inhibitors for 24 h in the presence or absence of AD-HGPC (300 nM) (*mean+/- SEM, N=3, n=6-9, *p<0.05, **p < 0.01*). **G.** AD-HGPC increases P-Akt expression. Immunoblots showing the increase of P-Akt expression after AD-HGPC (300 nM) treatment for 10 min on MDA-MB-435s and HEK-TRPV2 cells.

Figure 7

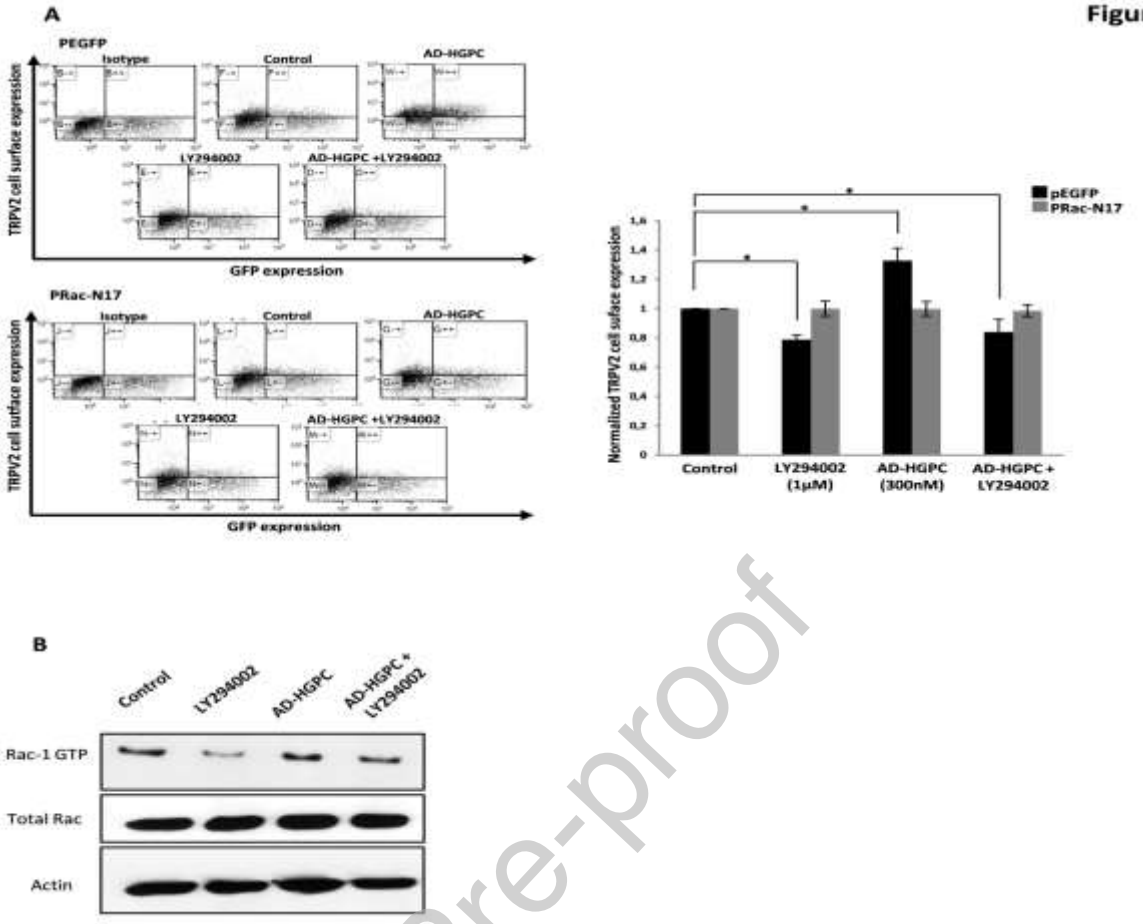

Figure 7: AD-HGPC and LPC induces translocation of TRPV2 to the plasma membrane by the PI3K/Akt/Rac1 pathway. **A**. P-RacN17-GFP, a dominant-negative plasmid of Rac1, blocks the translocation of the TRPV2 channel to the plasma membrane. The increase of TRPV2 plasma recruitment induced by AD-HGPC (300 nM) is abolished by pre-treatment of MDA-MB-435s cells with LY294002. Transfection with the P-RacN17-GFP plasmid abolished the PI3K activity with regard to the translocation of TRPV2 to the plasma membrane and the effect of the PI3K inhibitor LY294002 *(histograms showing mean +/- SEM, N=5, *p < 0.05)*. **B.** Immunoblot represents expression of Rac1 activity in MDA-MB-435s cells. The increase of Rac1-GTP expression induced by AD-HGPC is inhibited by LY294002.